Chance-Constrained Optimization of Infrastructure Resilience: A Utility-Driven Budget Allocation Framework

Tugce Uslu Aktas[a], Gino Lim[a,*], Jian Shi[b]

[a]*Department of Industrial and Systems Engineering, University of Houston, Houston, TX, USA*
[b]*Departments of Electrical and Computer Engineering & Engineering Technology, University of Houston, Houston, TX, USA*

Abstract

This paper presents a novel chance-constrained model to enhance infrastructure resilience in a stochastic environment under budget constraints. Our goal is to maximize resilience by accounting for the system's robustness and recovery capability, both of which are essential indicators of a resilient system. The uncertainty in functional degradation and recovery time of components is considered due to the uncertain intensity of adverse occurrences. The framework accommodates multiple distributional assumptions, including normal and uniform distributions, and integrates both linear and nonlinear utility functions to determine optimal trade-offs between reducing functional degradation and improving recovery. In addition, to efficiently solve the nonconvex utility formulation, a successive convex approximation algorithm is implemented, which significantly improves computational performance. The model is validated through three case studies (an illustrative system, a power transmission network, and a transportation network), demonstrating its applicability across different infrastructures. The results highlight the framework's ability to generate efficient budget allocation plans that maximize resilience while accounting for uncertainty in extreme events.

Keywords: Resilience, Resilience enhancement, Chance-Constrained Programming, Stochastic Programming, Resource allocation, Robustness, Recovery

1. Introduction

While events like earthquakes, floods, and other natural disasters occur with low frequency, their potential to significantly affect large populations highlights the importance of proactive planning and resilience. In 1994, the Northridge Earthquake in California led to both fatalities and injuries across the region (U.S. Geological Survey, 2024). Hurricane Katrina in 2005 brought about catastrophic destruction to certain regions of Louisiana and Mississippi, resulting in around 1800 deaths (Knabb et al., 2005). In 2021, Hurricane Ida led to the largest power outage ever recorded in Louisiana, with 200 million customer hours lost (Xu et al., 2024).

Resilience is a broad concept that has been used in a wide range of areas such as health-

*Corresponding author

Email addresses: tuslu@uh.edu (Tugce Uslu Aktas), ginolim@uh.edu (Gino Lim), jshi14@uh.edu (Jian Shi)

care, supply chain management, power systems, transportation, and telecommunications, to name a few. Quantifying system resilience provides valuable insights into a system's capacity to resist disruptions, recover from adverse conditions, and identify underlying vulnerabilities.

Studies related to resilience quantification metrics in the literature can be categorized into two main approaches: deterministic and stochastic. Some researchers have developed resilience metrics by considering deterministic system behavior, whereas other studies took uncertainty into account within the metric. The seminal work of Bruneau et al. (2003) is one of the earlier studies in the literature to measure resilience. They describe four dimensions of a resilient system: robustness, redundancy, resourcefulness, and rapidity. Reed et al. (2009) take into account time intervals in the resilience metric. Francis & Bekera (2014) describe a resilience metric considering absorptive capacity, adaptive capacity, restorative capacity as well as speedy recovery. Najarian & Lim (2019) introduce a framework to design resilience metrics and provide an assessment methodology based on experimental design methods. This quantitative assessment method enables a fair comparison of the effectiveness of the resilience metrics in the literature. Other studies propose optimization models aiming to maximize resilience under budget constraints (Ahmadian et al., 2020; Najarian & Lim, 2020).

Chance-constrained programming (CCP) is a stochastic programming framework that handles decision making under uncertainty and enables meeting constraints with a given probability. Significant progress has been made in the theoretical analysis and computational techniques for CCP (Charnes & Cooper, 1959; Pintér, 1989; Prékopa, 1973; Prékopa, 1995). Miller & Wagner (1965) study joint chance constraints, requiring all constraints to be satisfied simultaneously. Over the years, CCP has been applied in various areas, and different types of approaches and algorithms are offered to design efficient solutions to the problems such application areas include supply chain management (Bilsel & Ravindran, 2011), financial risk management and portfolio optimization (Ermoliev et al., 2000), power system operations (Wang et al., 2023), treatment planning in healthcare (Zaghian et al., 2018), transportation (Huang et al., 2023), and environmental management (Bavaghar Zaeimi & Abbas Rassafi, 2021), among others.

In this study, we introduce a novel chance-constrained model to strengthen resilience in a stochastic environment under budget constraints. The model maximizes infrastructure resilience by focusing on robustness and recovery ability, ensuring that resilience remains within the desired range after extreme events such as hurricanes or earthquakes through optimal budget allocation. We explore both linear and nonlinear utility functions to capture the optimal trade-off between functional degradation and recovery improvements for budget allocation decisions. Since the severity of adverse events is not known in advance, their impacts on functional degradation and recovery times are inherently uncertain. Accordingly, we use chance constraints to quantify the achieved confidence levels with which the resilience thresholds are met. A tractable deterministic equivalent optimization model is developed from chance constraints under certain conditions. In addition, a successive convex approximation approach is applied to handle non-convex utility functions by constructing convex surrogate problems. We further demonstrate that the proposed framework can be applied under different distributional assumptions, showing its capacity to operate under varying probabilistic settings.

The main contributions of this research to the literature can be stated as follows:

1) We characterize a novel chance-constrained model for resilience investment planning

with utility indifference by deriving distribution specific deterministic equivalents and explicit tractability conditions, and we propose a convex approximation approach for nonconvex preference extensions that preserves the probabilistic interpretation of the original model, validated against global optimization benchmarks.

2) We develop a unified chance-constrained allocation framework that jointly captures uncertainty in functional degradation and recovery time under limited budgets, yielding interpretable robustness and recovery confidence levels as decision-relevant performance measures.

3) We incorporate utility indifference preference representations to capture trade-offs between robustness and recovery within a single allocation model, enabling a systematic comparison across alternative preference specifications while maintaining a consistent probabilistic protection structure.

4) We demonstrate transferability and practical relevance through three case studies, showing how the proposed framework supports actionable budgeting insights and systematic sensitivity analysis across uncertainty conditions, risk levels, and preference settings.

The remainder of the paper is organized as follows. Section 2 reviews related work and positions our contribution. Section 3 introduces the proposed model, which incorporates budget constraints in the resilience enhancement process and applies a successive convex approximation to handle non-convex utility functions. Section 4 presents case studies from diverse systems to validate and demonstrate the applicability of the proposed model. Finally, Section 5 concludes the paper by summarizing the findings and offering recommendations for future research.

2. Related Work and Comparative Analysis

This section reviews closely related resilience planning studies and positions our contribution, with Table 1 summarizing representative work and modeling features. For example, Najarian & Lim (2020) allocate limited resources across components by selecting predefined enhancement alternatives for absorption and recovery using utility-shaped trade-offs and component criticality; however, their formulation optimizes a resilience metric under a budget without explicitly representing uncertainty or imposing chance constraints. Ren et al. (2017) propose a multi-objective model aligned with functionality, rapidity, and resourcefulness, with budgets enforced via life cycle cost; in contrast, our utility-based preference layer provides a compact calibration mechanism that allows the same allocation model to be reweighted across applications without modifying the underlying network formulation. Beyond deterministic allocation, uncertainty has been incorporated through fuzzy and stochastic programming in related domains, such as the two-stage stochastic Data Envelopment Analysis integrated model in a fuzzy environment for resilient supply chains proposed by Izadikhah et al. (2021). In energy system settings, probabilistic feasibility has been addressed in operational and microgrid contexts, including chance-constrained co-optimization of gas and power operations under renewable generation and demand uncertainty (Shabazbegian et al., 2021), distribution network resilience improvement under uncertain demand and renewable generation (Biswas et al., 2021), and nested mixed-integer linear programming model with probabilistic constraints for microgrid management (Park & Shin, 2022). Taken together, Table 1 highlights a persistent gap in the resilience allocation literature: many studies optimize resilience under a budget and then evaluate solutions under adverse scenarios, but

they typically do not impose probabilistic target attainment requirements for robustness and recovery within the optimization model. Consequently, the resulting allocations may either provide insufficient protection against uncertainty or require more spending than is actually needed.

To further motivate our uncertainty treatment, we next summarize how uncertainty enters resilience planning through component degradation and recovery. Two channels are considered: uncertain degradation that drives robustness losses and uncertain recovery durations that shape the recovery trajectory. On the robustness side, Panteli et al. (2017) map extreme weather intensity to component failure probabilities via fragility models and quantify system level impacts using a probabilistic assessment framework. On the recovery side, Arif et al. (2018) model uncertain repair times in a two-stage stochastic formulation that co-optimizes crew actions and network operations. Related restoration studies extend this line of work by integrating repair decisions with dynamic network reconfiguration and the dispatch of distributed energy resources (Shi et al., 2022), and by proposing sequential and two-stage stochastic formulations for crew dispatch and extreme weather driven restoration operations (Shuai et al., 2023; Hou et al., 2023). In a related direction, Ashokaraju et al. (2026) develop a distributionally robust chance-constrained model that provides probabilistic feasibility protection under distributional ambiguity.

Motivated by this literature, we formulate resilience enhancement as a risk-calibrated allocation problem in which uncertainty enters through two distinct channels of 1) component functional degradation and 2) component recovery time. The proposed CCP approach incorporates these uncertainties by imposing probabilistic constraints that ensure robustness and recovery targets are met with high probability. In this way, the proposed approach produces outputs that are directly interpretable for resilience planning by answering questions such as "how much budget is needed to reach a given confidence level?" and "how allocations shift as risk tolerance changes?", rather than only expected-performance reports.

In addition, degradation uncertainty and recovery time uncertainty are frequently handled in isolation, and reported results commonly rely on scenario summaries rather than outcome level reliability guarantees. To address this gap, we simultaneously model uncertainty in degradation amount and recovery time and use chance constraints to quantify the achieved confidence levels for meeting robustness and recovery targets.

This outcome level perspective also differentiates our results from prior work. Compared with expectation-based or scenario-based stochastic programming formulations, which typically optimize expected performance across sampled realizations, the proposed CCP model shifts the focus to outcome-level confidence by quantifying the probability of meeting robustness and recovery targets. This produces interpretable reliability style outcomes rather than expected-value summaries, which is consistent with resilience planning practice. Similarly, robust optimization (RO) can be particularly valuable when protection against severe adverse realizations is a priority. However, depending on the uncertainty set, RO may produce conservative solutions, especially for rare, high-impact hazards where full worst-case protection may be economically difficult to justify. In comparison, CCP offers a more balanced alternative by enabling the decision maker to control the acceptable level of risk through probabilistic constraints. Accordingly, CCP is particularly well suited to budget-limited resilience planning because it links investment decisions directly to the confidence of satisfying robustness and recovery requirements under uncertainty.

Reference	Modeling Approach		Uncertain Parameters		Considers Budget Constraints	Application Area
	Deterministic	Stochastic	Degradation Amount	Recovery Time		
Ahmadian et al. (2020)	+	–	–	–	+	supply chain and power networks
Najarian & Lim (2020)	+	–	–	–	+	power network
Shabazbegian et al. (2021)	–	+	–	–	–	gas and electricity networks
Park & Shin (2022)	–	+	–	–	–	power system
Fattahi et al. (2020)	–	+	+	+	–	supply chain network
Li et al. (2019)	+	+	–	+	+	transportation network
Zhang et al. (2018)	+	–	–	–	+	multi-infrastructure networks
This paper	–	+	+	+	+	power and transportation networks

Table 1: Comparison of this paper with the most relevant studies in the literature.

3. Mathematical Formulation

This section introduces the proposed model, which considers the uncertainty in the functional degradation amount and recovery time of components to enhance system resilience under budget limitations.

3.1. Mathematical Notation

The mathematical notation of the proposed model is provided below. Indices and Sets:

N : Set of system components, $i = \{1, 2, 3, \ldots, i_{\max}\} \in \mathbb{N}$

Parameters:

R_0 : The functionality level of the system prior to a disruption

t_d : The time when a disruptive event takes place, where $t_d \in [0, T]$

T : The time at which the system completes its recovery and returns to its initial functionality

F_d : System functionality level at time t_d

Q_d : A desired level of system functionality at time t_d, where $Q_d \in (0, 1]$

Q_t : A desired level of recovery time, representing the system's overall recovery duration, where $Q_t \in [t_d, T]$

k_i : scale factor linking the market value of the component V_i to the required investment, $i \in \mathbb{N}$

B : The total available budget

A_i : The amount of degradation in the functionality of component i before investment, $i \in \mathbb{N}$

T_i : Recovery time of component i before investment, $i \in \mathbb{N}$

λ_d : A weight coefficient reflecting the importance of robustness capability

λ_t : A weight coefficient reflecting the importance of recovery ability

Decision Variables:

y_i : The amount of budget allocated to component i, $i \in \mathbb{N}$

a_i : The percentage improvement of component i in absorption amount, $i \in \mathbb{N}$

r_i : The percentage improvement of component i in recovery time, $i \in \mathbb{N}$

α_d : Risk level for the robustness target

α_t : Risk level for the recovery target

3.2. Robustness and Recovery Ability

Robustness and recovery are key factors for measuring system resilience, with robustness referring to the ability to resist stress without major functional loss and recovery denoting the process of restoring normal performance (Bruneau et al., 2003). Figure 1 illustrates a resilience graph depicting the system's functionality levels over time, where an adverse event occurs at time t_d. In this mathematical model, we evaluate these two key abilities for each component of the system and establish desired levels for the components to enhance system resilience against adverse situations.

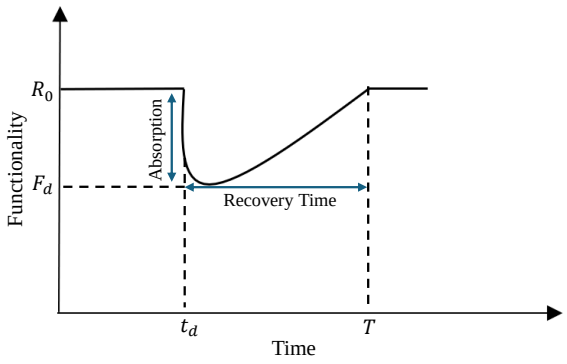

Figure 1: System Functionality Before and After a Disruption

3.3. Robustness Ability of a Component

The following formula is used to determine the amount of degradation for a component after the investment is made.

$$H_i(a_i) = A_i(1 - a_i) \tag{1}$$

where $H_i(a_i)$ is the amount of functional degradation of a component i after investment. To maintain system functionality (F_d) at a specific desired level (Q_d) for robustness ability, our goal is to ensure that F_d is greater than or equal to Q_d. Subsequently, assuming a linear degradation (Wang et al., 2024; Yodo & Wang, 2016), the F_d value after making the investment can be calculated as follows.

$$F_d = R_0 - H_i(a_i) \tag{2}$$

Therefore, the constraint can be expressed as given below.

$$R_0 - H_i(a_i) \geq Q_d \tag{3}$$

Alternatively, it can be expressed as:

$$H_i(a_i) \leq R_0 - Q_d \tag{4}$$

Satisfying this constraint after an extreme event cannot be guaranteed, even with sufficient funds to improve system components. In other words, encountering violations of constraints

due to unforeseen and extreme events is inevitable. Hence, we adopt chance constraints, which allow for a controlled level of constraint violation by incorporating uncertainty into the model. For robustness ability, maintaining the system functionality at a level with probability $(1 - \alpha_d)$ is desired.

$$P\{H_i(a_i) \leq R_0 - Q_d\} \geq 1 - \alpha_d \tag{5}$$

3.4. Recovery Ability of a Component

The following formula is used to calculate the recovery time after an investment.

$$L_i(r_i) = T_i(1 - r_i) \tag{6}$$

Q_t denotes the desired level for recovery ability of the system. Our objective is to keep the recovery time of the system component within a desired threshold, aiming to ensure that the recovery time $L_i(r_i)$ does not exceed (Q_t).

$$L_i(r_i) \leq Q_t \tag{7}$$

Maintaining this constraint reliably after an extreme event presents challenges, even when ample funding is available to recover and enhance system functionality. To ensure recovery capability, we aim to keep the system's recovery time at a certain desired level, achieving this with a probability of $(1 - \alpha_t)$.

$$P\{L_i(r_i) \leq Q_t\} \geq 1 - \alpha_t \tag{8}$$

3.5. Utility Function Integration

Various resilience enhancement actions may produce different effects on absorbability and recovery. If a_i or r_i is 0, it indicates no improvement in robustness or recovery, respectively. Conversely, if a_i and r_i are 1, the component can fully recover from the adverse event. Allocating all available funds to improve absorption could render the system unable to recover effectively. On the other hand, if all funds are directed toward enhancing recovery, the system may not be robust enough to withstand an event. Alternatively, improvements in the two capabilities may be achieved together. The relationship between the investment amount and (a_i, r_i) can be expressed using indifference curves, which in economics represent combinations of two goods that yield the same level of utility. Through indifference curves, the utility function $U(a, r)$ describes how the budget assigned to a component translates into improvements in its absorption and recovery. Table 2 presents the different types of utility functions in the literature. The value V_i reflects the market value of component i. If V_1 is much greater than V_2, the higher-value component requires more investment to achieve the same improvement. It is assumed that y_i is proportional to V_i, and this relationship is incorporated into the model through the scale factor k_i.

In our problem, the type of the utility function can affect the improvement levels for robustness and recovery ability. To reflect different priorities and model non-linear relationships between robustness and recovery, we explore different types of utility functions. It is worth noting that the appropriate utility function should be selected based on the specific relationship between robustness and recovery. For instance, a linear utility function assumes constant trade-offs between robustness and recovery. The Cobb-Douglas function captures

diminishing marginal returns, assuming both are necessary and can be substituted to some extent, while the CES function allows for varying degrees of substitution between robustness and recovery. The quasi-linear function places more emphasis on one objective, and the quadratic utility function models more complex and non-linear relationships, especially in scenarios involving risk aversion.

Utility Function	Formulation
Linear (Varian, 2010)	$U(a,r) = \dfrac{\beta_1 a + \beta_2 r}{k}$
Cobb–Douglas (Varian, 2010)	$U(a,r) = \dfrac{a^p r^{1-p}}{k}, \quad p < 1$
CES (Arrow et al., 1961)	$U(a,r) = \dfrac{C}{k}\left(\beta a^p + (1-\beta) r^p\right)^{\frac{1}{p}}$
Quadratic (De Luca, 2018)	$U(a,r) = \dfrac{b_0 + b_1 a + b_2 r - b_3 a^2 - b_4 r^2 - b_5 ar}{k}$
Quasi–Linear (Varian, 2010)	$U(a,r) = \dfrac{\gamma_1\, v(a) + \gamma_2\, r}{k}$

Table 2: Utility functions and their mathematical formulations.

3.6. Proposed CCP Model

$$\max\ \lambda_d(1-\alpha_d) + \lambda_t(1-\alpha_t) \tag{9}$$

s.t.

$$P\left\{\tilde{H}_i(a_i) \le R_0 - Q_d\right\} \ge 1-\alpha_d, \qquad \forall i \in \mathbb{N} \tag{10}$$

$$P\left\{\tilde{L}_i(r_i) \le Q_t\right\} \ge 1-\alpha_t, \qquad \forall i \in \mathbb{N} \tag{11}$$

$$\beta_{i1} a_i + \beta_{i2} r_i = y_i k_i, \qquad \forall i \in \mathbb{N} \tag{12}$$

$$\sum_{i=1}^{n} y_i \le B \tag{13}$$

$$y_i \ge 0, \qquad \forall i \in \mathbb{N} \tag{14}$$

$$0 \le a_i, r_i \le 1, \qquad \forall i \in \mathbb{N} \tag{15}$$

In the objective function (9), we aim to maximize the confidence levels $(1-\alpha_d)$ and $(1-\alpha_t)$ associated with robustness and recovery, respectively, which serve as probabilistic indicators of system resilience. Rather than optimizing average system performance, the proposed objective focuses on increasing the likelihood that predefined robustness and recovery requirements are satisfied under uncertainty. In this sense, the objective directly targets the risk of unacceptable outcomes, such as excessive functional degradation or delayed recovery beyond a prescribed deadline.

In practice, the objective allocates a fixed resilience investment budget to maximize the probability of meeting minimum robustness and recovery thresholds in the presence of uncertain degradation and recovery processes. Here, α_d and α_t represent the allowable violation probabilities for robustness and recovery constraints, so that $(1-\alpha_d)$ and $(1-\alpha_t)$

quantify the corresponding confidence levels. This formulation explicitly reflects decision makers' risk tolerance by controlling the acceptable likelihood of failing to meet critical performance requirements.

The weighting parameters λ_d and λ_t govern the trade-off between robustness and recovery when budget limitations prevent both confidence levels from being simultaneously maximized. In this way, the model determines how resources are prioritized between maintaining immediate post-event functionality and enabling faster recovery. Consequently, such a confidence-based objective provides an interpretable, risk-aware approach for allocating limited resources by directly reducing the probability of violating robustness and recovery thresholds, particularly under rare but high-impact disruptive events.

Constraint (10) guarantees that degradation does not exceed the allowable loss $(R_0 - Q_d)$, ensuring acceptable levels of functional degradation at time t_d. Constraint (11) ensures that the recovery time of each component remains below the acceptable threshold (Q_t), facilitating a timely return to normal operation.

Constraint (12) embeds the utility-based allocation structure by linking the allocated budget y_i to the attainable improvement levels in absorption and recovery, denoted by a_i and r_i, respectively. In the main formulation, a linear utility function is adopted, and accordingly Constraint (12) takes the form $\beta_{i1}a_i + \beta_{i2}r_i = y_i k_i$. Here, β_{i1} and β_{i2} are the coefficients of the linear utility function and describe how the allocated budget is translated into improvements in absorption and recovery. Under this relation, y_i determines the feasible combinations of a_i and r_i that can be attained for component i. Therefore, increasing improvement in one dimension requires a larger share of the allocated budget, which limits the attainable improvement in the other dimension. In this sense, the utility function acts as a trade-off structure between robustness and recovery enhancement decisions.

Moreover, constraint (12) should be interpreted jointly with constraints (10) and (11). While constraints (10) and (11) impose probabilistic performance requirements on absorption and recovery through the post-investment degradation and recovery expressions, constraint (12) restricts which combinations of a_i and r_i are attainable under the allocated budget. Hence, a_i and r_i are not chosen independently; their feasible values are determined simultaneously by the required resilience targets and the allocation of the available budget between absorption and recovery oriented improvements. The decision variables a_i, r_i, and y_i are therefore optimized jointly within a common feasible region. While the main formulation is based on a linear utility function, the alternative utility functions listed in Table 2 may also be adopted when different relationships between absorption and recovery are to be represented.

Constraint (13) restricts the budget allocated for enhancing system resilience. Constraint (14) reflects that y_i is nonnegative. Constraint (15) ensures that a_i and r_i are within the range of 0 to 1.

3.7. Deterministically equivalent convex model formulation of CCP

We construct a deterministically equivalent formulation of the proposed model by transforming the probabilistic constraints into tractable linear forms that can be solved using optimization techniques. This allows us to handle uncertainty explicitly while ensuring the model remains computationally efficient and solvable.

Due to the unpredictable nature of real-world events, both the functional degradation and recovery time are treated as uncertain parameters $(\tilde{A}_i, \tilde{T}_i)$. The new functional degradation

amount and recovery time, adjusted based on the applied improvements, can be denoted as follows:

$$\begin{aligned} \tilde{H}_i(a_i) &= \tilde{A}_i(1 - a_i) \\ \tilde{L}_i(r_i) &= \tilde{T}_i(1 - r_i) \end{aligned} \tag{16}$$

3.7.1. Convex reformulation of CCP under normal distribution

We begin this section by assuming that the uncertain parameters follow a normal distribution, as the central limit theorem suggests that the aggregation of multiple random errors leads to a normally distributed error (Agterberg, 2014; Montgomery & Runger, 2020). A normal distribution is also assumed for the repair time of failed power lines in the study by Ouyang et al. (2012). The following propositions highlight the key structural properties of the constraints under the normal distribution. Detailed proofs of Propositions 1 and 2 are provided in Appendices A and B, respectively.

Proposition 1. Under the assumption that the uncertain parameter is normally distributed, the feasible region corresponding to each chance constraint retains convexity for any α value in the interval [0, 0.5].

Corollary 1. The set of chance constraints produces a convex feasible region for all $\alpha \leq 0.5$, assuming the uncertainties follow a normal distribution.

$$\begin{aligned} P\left\{\tilde{H}_i(a_i) \leq R_0 - Q_d\right\} \geq 1 - \alpha_d, \quad \forall i \in \mathbb{N} \\ P\left\{\tilde{L}_i(r_i) \leq Q_t\right\} \geq 1 - \alpha_t, \quad \forall i \in \mathbb{N} \end{aligned} \tag{17}$$

Proof. Each constraint yields a convex feasible region for $\alpha \leq 0.5$ under normally distributed uncertainties, as stated in Proposition 1. Since the intersection of convex sets remains convex (Lagoa et al., 2005; Bazaraa et al., 2013), the feasible region of the chance constraints (5) and (8) is also convex.

Proposition 2. Assume random degradation amount $\tilde{H}_i(a_i)$ and recovery time $\tilde{L}_i(r_i)$ are normally distributed with mean $E(\tilde{H}_i(a_i))$ and $E(\tilde{L}_i(r_i))$, and standard deviation $\sigma(\tilde{H}_i(a_i))$ and $\sigma(\tilde{L}_i(r_i))$, respectively. Then, any feasible solution to constraints (18)–(19) below is also feasible for constraint (17).

$$E(\tilde{H}_i(a_i)) + \Phi^{-1}(1 - \alpha_d)\,\sigma(\tilde{H}_i(a_i)) \leq R_0 - Q_d, \qquad \forall i \in \mathbb{N} \tag{18}$$

$$E(\tilde{L}_i(r_i)) + \Phi^{-1}(1 - \alpha_t)\,\sigma(\tilde{L}_i(r_i)) \leq Q_t, \qquad \forall i \in \mathbb{N} \tag{19}$$

where, function $\Phi(\cdot)$ denotes the cumulative distribution function of a standard normal probability density.

Hence, we have a convex version of CCP under normal distribution when $\alpha \leq 0.5$ follows.

$$\begin{aligned}
&\max\ \lambda_d(1-\alpha_d) + \lambda_t(1-\alpha_t) \\
&\text{s.t.}\quad E(\tilde{H}_i(a_i)) + \Phi^{-1}(1-\alpha_d)\sigma(\tilde{H}_i(a_i)) \leq R_0 - Q_d, \quad \forall i \in \mathbb{N} \\
&\qquad E(\tilde{L}_i(r_i)) + \Phi^{-1}(1-\alpha_t)\sigma(\tilde{L}_i(r_i)) \leq Q_t, \quad \forall i \in \mathbb{N} \\
&\qquad \beta_{i1}a_i + \beta_{i2}r_i = y_i k_i, \quad \forall i \in \mathbb{N} \\
&\qquad \sum_{i=1}^{n} y_i \leq B \\
&\qquad y_i \geq 0, \quad \forall i \in \mathbb{N} \\
&\qquad 0 \leq a_i, r_i \leq 1, \quad \forall i \in \mathbb{N} \\
&\qquad \alpha_d, \alpha_t \leq \frac{1}{2}
\end{aligned} \tag{20}$$

The difficulty in finding the optimal value of α arises because $\Phi^{-1}(y)$ is a monotonically increasing function of y. To address this issue, we rewrite the objective function as follows:

$$\max\ \lambda_d\Phi^{-1}(1-\alpha_d) + \lambda_t\Phi^{-1}(1-\alpha_t) \tag{21}$$

Let $G_{(\alpha)} = \Phi^{-1}(1-\alpha)$ denote a newly introduced variable for a in the set $\{\alpha_d, \alpha_t\}$, allowing us to express the proposed optimization model as follows:

$$\begin{aligned}
&\max\ \lambda_d G_{(\alpha_d)} + \lambda_t G_{(\alpha_t)} \\
&\text{s.t.}\quad E(\tilde{H}_i(a_i)) + G_{(\alpha_d)}\sigma(\tilde{H}_i(a_i)) \leq R_0 - Q_d, \quad \forall i \in \mathbb{N} \\
&\qquad E(\tilde{L}_i(r_i)) + G_{(\alpha_t)}\sigma(\tilde{L}_i(r_i)) \leq Q_t, \quad \forall i \in \mathbb{N} \\
&\qquad \beta_{i1}a_i + \beta_{i2}r_i = y_i k_i, \quad \forall i \in \mathbb{N} \\
&\qquad \sum_{i=1}^{n} y_i \leq B \\
&\qquad y_i \geq 0, \quad \forall i \in \mathbb{N} \\
&\qquad 0 \leq a_i, r_i \leq 1, \quad \forall i \in \mathbb{N} \\
&\qquad G_{(\alpha_d)}, G_{(\alpha_t)} \geq 0
\end{aligned} \tag{22}$$

3.7.2. Convex reformulations of CCP under uniform distribution

We continue our exercise under a uniform distribution assumption because it is a simple probabilistic model with equal probability across its range (Montgomery & Runger, 2020; Jayakumar & Sankaran, 2016). Its simplicity and uniformity make it effective for comprehensively testing all possible outcomes by addressing uncertainty. Song & Li (2022) also adopt a uniform distribution to model the maximum performance degradation under uncertainty. The following propositions present key structural properties of the constraints under the uniform distribution. Appendices C and D are provided for proofs of Propositions 3 and 4, respectively.

We employ the method proposed by Calafiore & Ghaoui (2006) for uniform distributions over an ellipsoidal support.

Proposition 3. For any $\alpha \leq 1/2$, the feasible region of the chance constraints is convex, provided that the uncertain distributions $A_i - E(A_i)$ and $T_i - E(T_i)$ follow a uniform distribution within the ellipsoid defined by $\varepsilon = \{\xi = Qz : \|z\| \leq 1\}$.

Corollary 2. The convexity of the feasible region defined by the chance constraints is preserved if $A_i - E(A_i)$ and $T_i - E(T_i)$ follow a uniform distribution over the ellipsoid $\varepsilon = \{\xi = Qz : \|z\| \leq 1\}$, for any risk level $\alpha \leq 1/2$.

Proof. Using a similar argument as in the proof of Corollary 1, this result stems from the principle that the intersection of convex sets remains convex (Bazaraa et al., 2013). Consequently, the feasible region of chance constraints remains convex under the given assumption.

Proposition 4. Let $A_i - \mathbb{E}(A_i)$ and $T_i - \mathbb{E}(T_i)$ be uniformly distributed within the ellipsoid $\mathcal{E} = \{\xi = Qz : \|z\| \leq 1\}$, where $Q = \nu\Gamma_f$ and $\nu = \sqrt{n+3}$, with $\Gamma \succ 0$. For any $\alpha \in (0, 0.5]$, the chance constraint can be equivalently expressed as the following convex second-order cone constraint:

$$E(\tilde{H}_i(a_i)) + \nu\sqrt{\Psi^{-1}_{\text{beta}}(1-2\alpha_d)}\,\sigma(\tilde{H}_i(a_i)) \leq R_0 - Q_d, \qquad \forall i \in \mathbb{N} \tag{23}$$

$$E(\tilde{L}_i(r_i)) + \nu\sqrt{\Psi^{-1}_{\text{beta}}(1-2\alpha_t)}\,\sigma(\tilde{L}_i(r_i)) \leq Q_t, \qquad \forall i \in \mathbb{N} \tag{24}$$

where $\Psi_{\text{beta}}(\cdot)$ denotes the cumulative distribution function of a Beta probability density function with parameters $1/2$ and $n/2+1$.

Hence, under a uniform distribution, we propose the following nonlinear optimization model to enhance system resilience. As $\Psi^{-1}_{\text{beta}}(y)$ is a monotonically increasing function of y, the proposed optimization model can be redesigned as given below.

$$\begin{aligned}
\max \quad & \lambda_d k(\alpha_d) + \lambda_t k(\alpha_t) \\
\text{s.t.} \quad & E(\tilde{H}_i(a_i)) + \sqrt{k(\alpha_d)}\,\sigma(\tilde{H}_i(a_i)) \leq R_0 - Q_d, && \forall i \in \mathbb{N} \\
& E(\tilde{L}_i(r_i)) + \sqrt{k(\alpha_t)}\,\sigma(\tilde{L}_i(r_i)) \leq Q_t, && \forall i \in \mathbb{N} \\
& \beta_{i1}a_i + \beta_{i2}r_i = y_i k_i, && \forall i \in \mathbb{N} \\
& \sum_{i=1}^{n} y_i \leq B \\
& y_i \geq 0, && \forall i \in \mathbb{N} \\
& 0 \leq a_i, r_i \leq 1, && \forall i \in \mathbb{N} \\
& k_{\alpha_d}, k_{\alpha_t} \geq 0 \\
\text{where} \quad & k_\alpha = \nu^2 \Psi^{-1}_{\text{beta}}(1-2\alpha), \quad \alpha \in \{\alpha_d, \alpha_t\}.
\end{aligned} \tag{25}$$

3.8. Successive Convex Approximation for Non-convex Utility Functions

For convex utility functions, the global optimum can be guaranteed due to their well-behaved structure. In contrast, the Cobb–Douglas and CES utility functions are inherently nonlinear and non-convex. Their non-convex structure makes them difficult or computationally expensive to solve directly using global commercial solvers. Therefore, we employ a successive convex approximation (SCA) method (Palomar, 2025; Scutari & Sun, 2018), utilizing a first-order Taylor expansion, to solve the model with non-convex utility functions.

Algorithm 1 outlines the detailed procedure of the applied method with the CES utility function. Within the optimization model, the non-convex utility function is linearized

through a first-order Taylor expansion at each SCA iteration, whereas the chance-constrained components are convex and thus left unchanged. The algorithm solves the convexified problem, updates the decision variables using a diminishing step size, and repeats this process until convergence. The stopping criterion is satisfied when the maximum change in decision variables between two consecutive iterations becomes smaller than a predefined tolerance, indicating that the solution has stabilized.

Algorithm 1 Successive Convex Approximation

Require: Initial point $x_0 = (a^0, r^0, y^0) \in X$, and a step-size sequence $\{\gamma_k\}$ with $\gamma_0 = 1$; inverse step variable $\text{invGam} = 1/\gamma_0$; step-size decay $\varepsilon_{\text{step}} > 0$; tolerance $\varepsilon_{\text{tol}} > 0$.

Ensure: Converged solution x^k.

1: Initialize $k \leftarrow 0$

2: **repeat**

3: Step 1: Construct the convex surrogate of the CES utility function at the current iterate $x^k = (a^k,\, r^k,\, y^k)$ via first-order Taylor expansion.

$$f(a, r, y) = \left[\beta a^\rho + (1-\beta) r^\rho\right]^{1/\rho} - k\, y = 0$$

$$\left.\frac{\partial f}{\partial a}\right|_{x^k} = \beta\,(a^k)^{\rho-1}\left[\beta(a^k)^\rho + (1-\beta)(r^k)^\rho\right]^{\frac{1}{\rho}-1},$$

$$\left.\frac{\partial f}{\partial r}\right|_{x^k} = (1-\beta)\,(r^k)^{\rho-1}\left[\beta(a^k)^\rho + (1-\beta)(r^k)^\rho\right]^{\frac{1}{\rho}-1},$$

$$\left.\frac{\partial f}{\partial y}\right|_{x^k} = -\,k.$$

$$\tilde{f}(a, r, y;\, x^k) \approx f(a^k, r^k, y^k) + \nabla f(a^k, r^k, y^k)^\top \begin{bmatrix} a - a^k \\ r - r^k \\ y - y^k \end{bmatrix} \;=\; 0$$

4: Step 2: Solve the surrogate convex problem to obtain an intermediate solution $\hat{x}^{k+1}$.
Use the optimization models (22) and (25), corresponding to the normal and uniform distribution cases, respectively, when incorporating non-convex utility functions.
Replace the non-convex utility constraint with its convex surrogate using a first-order Taylor expansion, and keep all other constraints unchanged.

5: Step 3: Update the next iterate.

$$x^{k+1} = x^k + \gamma_k\big(\hat{x}^{k+1} - x^k\big)$$

6: Step 4: Diminishing step-size update.

$$\gamma_{k+1} = \frac{1}{\text{invGam}}, \qquad \text{invGam} \leftarrow \text{invGam} + \varepsilon_{\text{step}}$$

7: Step 5: Increment the iteration counter. $k \leftarrow k + 1$

8: **until** $\|x^k - x^{k-1}\| \le \varepsilon_{\text{tol}}$

4. Case Study Applications

To demonstrate the range of applicability of the proposed chance constrained allocation framework, we present three case study applications. Case 1 provides an illustrative benchmark to explain model behavior under alternative distributional assumptions, Case 2 evaluates scalability and interpretability on a realistic and larger scale power transmission test

network, and Case 3 demonstrates transferability to transportation networks with damage state based performance representations. Taken together, these applications show that the same modeling core can be applied across different infrastructure contexts through domain specific parameterization.

4.1. Case 1: Illustrative System

We examine a system consisting of 10 components. We assume that the functional degradation amounts and recovery times of the components follow both normal and uniform distributions. The market value, representing the cost to buy or sell each component, is assumed to be as shown in Table 3. We use the utility functions, combined with the market value of each component, in the model to allocate funds to each component. It is assumed that scale factor $k_i = \frac{1}{V_i}$, meaning that investment is made in proportion to the component's value. We obtained the results by considering the uncertain parameters of the proposed model, namely the functional degradation amount and recovery time. The distribution parameters, assumed for illustrative modeling purposes, are provided in Appendix E. We assume that the initial resilience of the system is 1 ($R_0 = 1$). The robustness threshold of 0.7 (Q_d) is chosen to maintain the system's functionality slightly above the average value (0.5). The recovery time is considered as 50 days (Q_t) since critical facilities typically recover within weeks to months. As outlined in the guidance provided by NIST, recovery targets for critical infrastructure such as wastewater systems often aim for up to 90% functionality restoration within 4 to 8 weeks (National Institute of Standards and Technology, 2017).

Note that the desired level of robustness is between 0 and 1, as system resilience is gauged within this range according to the resilience graph. For example, if the desired robustness level at time t_d is 1, it implies that we anticipate the system's functionality will remain fully intact at 1 at time t_d, unaffected by any adverse events, indicating a very high robustness ability. In other words, a robustness level closer to 1 indicates a more robust system, whereas a level closer to 0 suggests a lower robustness ability. For assessing recovery ability, we consider the total number of days required to restore the system. For this numerical analysis, we anticipate that the recovery time will be less than 50 days with a specified probability. The weight coefficients for robustness and recovery ability are assigned equal importance in the objective function, each set at 0.5.

Component	$i=1$	$i=2$	$i=3$	$i=4$	$i=5$	$i=6$	$i=7$	$i=8$	$i=9$	$i=10$
Market Value ($)	7,000	3,000	10,000	15,000	30,000	5,000	20,000	2,000	3,000	20,000

Table 3: Market value of the components (V_i).

4.1.1. Results

First, we employ a linear utility function, based on the assumption that the relationship between the absorption amount (a) and recovery time (r) is linear. The coefficients of the linear utility function are set to 0.5 for both β_{i1} and β_{i2}.

Table 5: Sensitivity analysis for the linear utility function under normal distribution, with results reported as changes relative to the base case.

Decision-maker parameters									
	Base	B (0.9B/1.1B)		λ_d (0.25/0.75)		Q_d (0.65/0.75)		Q_t (45/55)	
Metric	value	$\Delta-$	$\Delta+$	$\Delta-$	$\Delta+$	$\Delta-$	$\Delta+$	$\Delta-$	$\Delta+$
Achieved robustness confidence $(1-\alpha_d)$	1.00	-0.42	0.00	-0.50	0.00	0.00	-0.44	-0.25	0.00
Achieved recovery confidence $(1-\alpha_t)$	0.50	0.00	+0.25	+0.35	0.00	+0.18	0.00	0.00	+0.17
Top-5 budget share	82%	0.00	0.00	+0.01	0.00	0.00	0.00	0.00	0.00
Average robustness improvement	0.56	-0.09	+0.03	-0.10	0.00	-0.04	0.00	-0.07	+0.03
Average recovery improvement	0.33	0.00	+0.06	+0.09	0.00	+0.04	0.00	+0.07	-0.02
Robustness budget share	65%	-0.04	-0.04	-0.11	0.00	-0.05	0.00	-0.08	+0.02
Recovery budget share	35%	+0.04	+0.04	+0.11	0.00	+0.05	0.00	+0.08	-0.02

Uncertainty parameters					
	Base	μ_A $(-10\%/+10\%)$		μ_T $(-10\%/+10\%)$	
Metric	value	$\Delta-$	$\Delta+$	$\Delta-$	$\Delta+$
Achieved robustness confidence $(1-\alpha_d)$	1.00	0.00	-0.06	0.00	-0.20
Achieved recovery confidence $(1-\alpha_t)$	0.50	+0.05	0.00	+0.17	0.00
Top-5 budget share	82%	0.00	0.00	0.00	0.00
Average robustness improvement	0.56	0.00	0.00	+0.03	-0.07
Average recovery improvement	0.33	+0.01	0.00	-0.02	+0.06
Robustness budget share	65%	-0.02	0.00	+0.02	-0.07
Recovery budget share	35%	+0.02	0.00	-0.02	+0.07

Component	$i=1$	$i=2$	$i=3$	$i=4$	$i=5$	$i=6$	$i=7$	$i=8$	$i=9$	$i=10$
a_i	0.54	0.42	0.60	0.69	0.46	0.56	0.63	0.71	0.45	0.56
r_i	0.50	0.33	0.38	0.41	0.29	0.33	0.17	0.55	0.09	0.29
y_i (\$)	3,628	1,134	4,872	8,248	11,357	2,245	8,004	1,259	817	8,436

Table 4: Percentage improvement in absorption amount (a_i) and recovery time (r_i), and investment amount (y_i) for each component under linear utility and normal distribution with a total budget of \$50,000.

Table 4 displays detailed results from considering the linear utility function under the budget constraint of \$50,000. The investment amount, percentage improvement in robustness, and percentage improvement in recovery time for each component are determined with confidence levels of 0.99 for system robustness and 0.50 for system recovery, where the confidence level is defined as $1-\alpha$. Figure 8 visualizes the component-level post-allocation functionality outcomes under the selected budget, with the detailed case-specific interpretation reported in the Appendix F.

Table 5 summarizes the sensitivity results for the linear utility setting by changing one input at a time and reporting all outcomes relative to the base case. We vary key decision maker inputs, including the total budget level, the robustness weight, and the robustness and recovery performance targets. We also test uncertainty inputs by shifting the mean level of the degradation distribution and the mean level of the recovery time distribution by $\pm 10\%$.

The results indicate a clear robustness recovery trade-off that is primarily driven by de-

cision maker inputs. Budget primarily determines how much confidence can be achieved, and limited budgets force a robustness recovery trade-off. In our results, cutting the budget reduces the ability to meet the robustness target with high confidence, whereas increasing the budget is first used to improve recovery performance rather than further increasing robustness. This occurs because robustness confidence is already near its maximum in the base case, so additional budget is more effective when directed to recovery.

The objective function uses two normalized weights that jointly set the relative importance of robustness versus recovery. When the weights shift emphasis toward recovery, achieved recovery confidence increases while achieved robustness confidence decreases, showing that the optimizer reallocates the limited budget in line with these stated priorities. Importantly, the weight pair is the main lever for encoding robustness recovery preference: shifting weight toward robustness increases robustness oriented spending and average robustness improvement, whereas shifting weight toward recovery increases the recovery budget share and average recovery improvement, typically at the expense of robustness outcomes. Within the range from 0.50 to 0.75, the results remain unchanged because robustness confidence is already near its maximum in the base solution, so increasing the robustness weight does not change the optimal investment set.

Increasing Q_d makes the robustness requirement more stringent, which lowers the achieved robustness confidence and reduces average robustness improvement because the model must allocate limited resources to meet a higher robustness threshold under uncertainty. On the other hand, relaxing Q_t makes the recovery requirement easier to satisfy, leading to higher achieved recovery confidence and allowing the model to reallocate effort toward other objectives. The practical implication is that Q_d and Q_t should be selected to reflect minimum acceptable service levels and recovery expectations: stricter targets directly reduce the probability of meeting them unless additional budget is provided, while looser targets free resources and increase the likelihood of compliance.

To assess sensitivity to uncertainty, we perturb the mean level of the underlying degradation and recovery time distributions by $\pm 10\%$ while keeping the decision maker parameters fixed. Increasing the degradation mean represents a harsher post event damage environment, whereas increasing the recovery time mean represents a slower recovery environment on average.

The uncertainty results are directional and economically intuitive. A higher recovery time mean has a stronger impact on the solution, reducing achieved robustness confidence and shifting spending toward recovery, as reflected by an increase in the recovery budget share and a decrease in the robustness budget share. In contrast, changes in the degradation mean produce milder effects, with only small movements in the reported metrics and budget shares, because the base solution already meets the robustness requirement with very high confidence and small shifts in average degradation do not substantially change the binding constraints or the optimal investment set. Overall, increasing the degradation mean represents a more severe damage regime, which may stem from a stronger extreme event, longer exposure, or a weaker pre-event condition of components due to aging or deferred maintenance. Increasing the recovery time mean represents a more challenging recovery regime driven by post-event constraints, including limited repair crews, supply chain delays, restricted site access, and system wide disruptions that slow down recovery across multiple components. From a planning perspective, these scenarios capture how both hazard characteristics and underlying

Table 6: Sensitivity of results to utility-function choice under normally distributed uncertainty.

Utility	Level	Parameters	Trade-off index	Average improvement		Achieved confidence	
				Robustness	Recovery	Robustness	Recovery
Linear (β_1, β_2)	low	(0.25,0.75)	0.33	0.59	0.40	1.00	0.80
	base	(0.50,0.50)	1.00	0.56	0.33	1.00	0.50
	high	(0.75,0.25)	3.00	0.46	0.35	0.50	0.60
Cobb–Douglas (p)	low	(0.25)	0.33	0.59	0.41	1.00	0.94
	base	(0.50)	1.00	0.59	0.35	1.00	0.59
	high	(0.75)	3.00	0.49	0.33	0.77	0.50
CES (β, p)	low	$(0.25, 0.50)$	0.33	0.59	0.34	1.00	0.52
	base	$(0.50, 0.50)$	1.00	0.59	0.41	1.00	0.82
	high	$(0.75, 0.50)$	3.00	0.48	0.33	0.67	0.50
Quadratic (b_3, b_4)	low	(0.50,1.00)	0.50	0.59	0.51	1.00	1.00
	base	(0.75,0.75)	1.00	0.59	0.48	1.00	0.98
	high	(1.00,0.50)	2.00	0.51	0.56	0.91	1.00
Quasi-linear (γ_1, γ_2)	low	(0.40,0.80)	0.50	0.59	0.39	1.00	0.74
	base	(0.50,0.50)	1.00	0.59	0.52	1.00	1.00
	high	(0.80,0.40)	2.00	0.50	0.56	0.86	1.00

Utility	Usage (when to prefer)
Linear	Fixed-weight aggregation with constant marginal trade-offs.
Cobb–Douglas	Joint improvement emphasis; poor performance in one dimension strongly limits utility.
CES	Tunable substitutability allowing partial compensation.
Quadratic	Penalizes large deviations below targets (risk-averse).
Quasi-linear	Baseline requirement in one dimension; nonlinear gain in the other.

asset conditions shape resilience outcomes and the resulting allocation between robustness focused and recovery focused actions. In addition, the budget split is very similar across all cases, with the top five components receiving about 82% of the total budget, showing that the solution keeps prioritizing a small set of critical components even when parameters change.

Decision makers may interpret Table 5 as a map of high impact drives and scenario risks. Budget, weight settings on the objective function, and performance targets directly control how the model prioritizes robustness versus recovery and therefore drive the largest shifts in achieved confidence levels and average improvements. At the same time, uncertainty shifts in the damage and recovery time means can noticeably lower achieved confidence and reallocate budget toward the more challenging requirement. Practically, this suggests that both careful selection of targets and weights and testing the recommended allocations under plausible hazard severity and asset condition scenarios are needed to produce resilient and defensible investment plans.

Table 6 shows how sensitive the model's outcomes are to the choice of utility function under normally distributed uncertainty. In our model, the utility function combines each component's robustness and recovery improvements into a single decision rule that guides budget allocation. When the budget is limited, it specifies how marginal gains are valued

across the two dimensions and thus shapes the robustness recovery trade-off under the assumed uncertainty.

In practice, the choice of utility structure depends on the planning context and the decision environment. Linear utility can be a reasonable starting point in capital budgeting and asset management settings where priorities are expressed as fixed weights, yielding allocations that are straightforward to interpret. Cobb–Douglas can be a useful choice for critical services such as emergency response, hospital operations, and port or terminal continuity, especially when balanced performance is emphasized and limited compensation between robustness and recovery is desired. CES may be preferred in settings such as energy systems and ports when stakeholders accept trade-offs yet disagree on substitutability; tuning its parameters provides a practical way to probe the implied compensation across dimensions. When large deviations from targets are viewed as unacceptable, a quadratic utility offers a practical way to encode increasing marginal penalties for falling below the target. Quasi-linear utility is often useful for policies that prioritize feasibility against a minimum threshold first, and then allocate remaining budget to improve the secondary dimension.

After selecting a utility form, parameter selection sets the implied marginal rate of substitution between robustness and recovery, i.e., the recovery gain the decision maker is willing to give up to obtain an additional unit of robustness under a tight budget. In our formulation, the trade-off index summarizes the relative investment intensity of robustness versus recovery. Values below one indicate that robustness improvement is cheaper per unit than recovery, a value of one indicates comparable intensities, and values above one indicate that robustness improvement is more investment intensive. Accordingly, the low, base, and high settings in Table 6 progress from relatively cheaper robustness (low), to comparable intensities (base), to relatively more expensive robustness (high). These settings represent different realistic cases for how cost effective robustness versus recovery investments are at the component level. The low setting corresponds to assets where robustness is relatively easy to improve, meaning that low-cost upgrades can noticeably reduce failure risk (e.g., replacing weak parts or adding basic protection). The high setting corresponds to assets where additional robustness improvement is costly and brings limited benefit, so it can be better to emphasize faster recovery (e.g., keeping spare parts ready or having repair crews on standby).

It is important to note that the objective-function coefficients and the utility parameters play distinct roles in the model. Objective function coefficients should be adjusted to reflect changes in policy priorities, i.e., the relative value assigned to robustness versus recovery in the overall objective. By contrast, utility parameters should be adjusted to reflect changes in implementation conditions that affect how budget converts into component level improvements, i.e., the relative investment intensity of robustness versus recovery. For example, if an agency places greater emphasis on reducing outage duration, it should increase the recovery weight in the objective; if, instead, repair resources become harder to procure during storm season, it should increase the recovery side investment intensity in the utility parameters.

4.2. Case 2: Power System

We conducted a case study on a reduced 29-bus version of the Great Britain transmission network (Panteli et al., 2017) (see Figure 2). This case study aims to validate the proposed model by evaluating its performance in a real-world scenario, maximizing system resilience against an adverse event through the optimal allocation of the budget among transmission

lines. This network includes 29 nodes, 98 overhead transmission lines in a double circuit configuration, and a single circuit transmission line connecting nodes 2 and 3. The double circuits are assumed to be on the same tower. In this study, each route within the network is treated as a component of the system. Thus, the total system consists of 50 components, including 49 double-circuit transmission lines and 1 single-circuit transmission line.

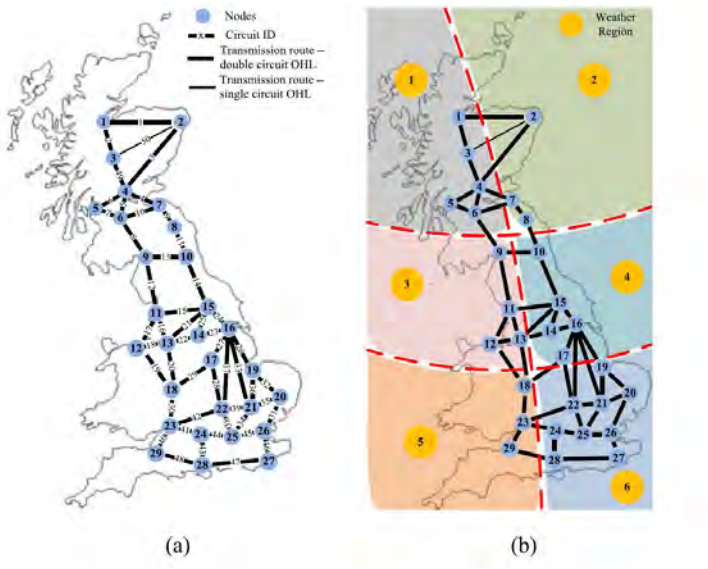

Figure 2: The simplified 29-bus model of the Great Britain transmission network: a) The transmission network layout. b) Weather regions corresponding to the network (Panteli et al., 2017).

4.2.1. Functional Degradation Amount

To assess the functional degradation of transmission lines, we use the fragility curve, which represents the probability of failure of a structure or its components. Figure 3 presents the fragility curve of transmission lines, taking into account both the robust and base cases.

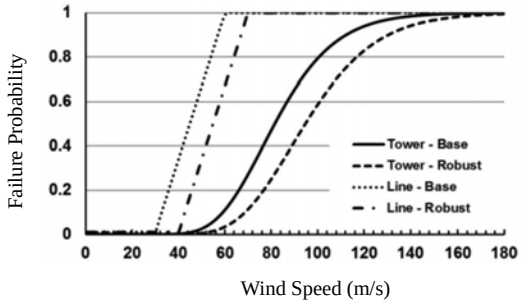

Figure 3: Wind fragility curves (Panteli et al., 2017).

We generate data using WebPlotDigitizer (Rohatgi, 2024) in order to extract samples from the wind fragility curve for transmission lines (base case). Assuming a uniform distribution, we calculate the mean and standard deviation based on the samples taken from the

fragility curve. Consequently, the functional degradation amount of the transmission lines follows a uniform distribution with a mean of 0.512 (A_{mean}) and a standard deviation of 0.284 (A_{sd}). The functional degradation amount is calculated based on the components of wind speed impact as follows.

$$A_{i,\text{mean}} = \begin{cases} P_L, & \text{if } w_{\max} < w_{\text{critical}} \\ k_1 * A_{\text{mean}}, & \text{if } w_{\text{critical}} \leq w_{\max} < w_{\text{collapse}} \\ 1, & \text{if } w_{\max} \geq w_{\text{collapse}} \end{cases} \tag{26}$$

where P_L is the functional degradation amount for good weather conditions, set as 1×10^{-2}. w_{critical} and w_{collapse} are 30 m/s and 60 m/s, respectively (Panteli et al., 2017). If the wind speed is between w_{critical} and w_{collapse}, coefficient k_1 is utilized, where $k_1 \sim U(0.5, 1.5)$. Hourly wind speed patterns over the 168-hour period were taken from Panteli et al. (2017), with the maximum wind speed recorded as $w_{\max} = 40\,\text{m/s}$.

A similar approach is adopted to obtain the standard deviation of the functional degradation amount for each component with respect to wind profiles.

$$A_{i,\text{sd}} = \begin{cases} P_L, & \text{if } w_{\max} < w_{\text{critical}} \\ k_2 \cdot A_{\text{sd}}, & \text{if } w_{\text{critical}} \leq w_{\max} < w_{\text{collapse}} \\ 1, & \text{if } w_{\max} \geq w_{\text{collapse}} \end{cases} \tag{27}$$

where random values of $k_2 \sim U(0.8, 1.2)$ are taken from the predetermined range.

4.2.2. Recovery time

We assume the recovery time of transmission lines is modeled by a uniform distribution T$\sim U(8, 12)$. Therefore, the mean and standard deviation of the recovery time for transmission lines can be obtained as 10 (T_{mean}) and 1.15 (T_{sd}), respectively, which is consistent with the range found in other studies (Panteli et al., 2017; Lindsey, 2015). Under different weather conditions for each component, the mean and standard deviation of the recovery time can be determined as follows. The formulations of $T_{i,\text{mean}}$ and $T_{i,\text{sd}}$ are modified from the recovery time formulation for transmission lines in Panteli et al. (2017), where k_3, k_4, and the thresholds of $w_{\max}$ were determined based on the National Grid.

$$T_{i,\text{mean}} = \begin{cases} T_{\text{mean}}, & w_{\max} \leq 20 \\ k_3 \cdot T_{\text{mean}}, & 20 < w_{\max} \leq 40 \\ k_4 \cdot T_{\text{mean}}, & 40 < w_{\max} \leq 60 \end{cases} \tag{28}$$

where $k_3 \sim U(2, 4)$ and $k_4 \sim U(5, 7)$ are uniformly distributed random variables within their defined intervals.

$$T_{i,\text{sd}} = \begin{cases} T_{\text{sd}}, & w_{\max} \leq 20 \\ k_5 \cdot T_{\text{sd}}, & 20 < w_{\max} \leq 40 \\ k_6 \cdot T_{\text{sd}}, & 40 < w_{\max} \leq 60 \end{cases} \tag{29}$$

where $k_5 \sim U(1.5, 3.5)$ and $k_6 \sim U(4.5, 6.5)$ are uniformly distributed random variables within their given ranges.

4.2.3. The cost of transmission lines

We incorporate the transmission line costs (V_i) into the utility functions using a scale factor (k_i), assuming that $k_i = \frac{1}{V_i}$. Table 7 outlines the components of transmission line costs along with the capital cost. The following equation is defined so as to calculate the cost of transmission lines.

$$\text{TransmissionLineCost}_i = \text{Capital Cost} \times L_i \tag{30}$$

where L_i represents the length of the transmission line (in miles) for each component. Since there is no information about the length of the transmission lines for Figure 6, the lengths are randomly assigned between 10 and 50 miles.

Cost Elements				Total (Capital) Cost ($M/mile)
Materials ($M/mile)	Labor ($M/mile)	ROW ($M/mile)	Substation ($M/mile)	
2.291	0.428	0.154	1.024	3.898

Table 7: Components of transmission line costs (DeSantis et al., 2021).

4.2.4. Results

We present the results of the case study using linear, quasi-linear, and nonlinear utility functions under different budget constraints. We consider three scenarios for linear utility functions. First, the desired levels for the robustness and recovery ability of the components are set to 0.7 (on a scale from 0 to 1) and 20 hours, respectively, which is considered the base case scenario. Then, we analyze the results when these limits are loosened by 20% (desired level for the robustness: 0.56, desired level for the recovery: 24 hours) and when they are tightened by 20% (desired level for the robustness: 0.84, desired level for the recovery: 16 hours). Detailed results based on the mathematical model with the linear utility function are provided in Table 8.

Budget Limitation ($B)	Confidence Levels $(1-\alpha)$					
	Base Case		Loosened levels by 20%		Tightened levels by 20%	
	Robustness Ability	Recovery Ability	Robustness Ability	Recovery Ability	Robustness Ability	Recovery Ability
$1.0	–	–	0.51	0.56	–	–
$1.5	–	–	0.59	1.00	–	–
$2.0	0.51	0.62	0.77	1.00	–	–
$2.5	0.59	1.00	0.99	1.00	–	–
$3.0	0.84	1.00	1.00	1.00	–	–
$3.5	1.00	1.00	1.00	1.00	0.55	1.00
$4.0	1.00	1.00	1.00	1.00	1.00	1.00

Note: "–" indicates that no feasible solution exists under the given budget.

Table 8: Robustness and Recovery Abilities under Different Budget Limitations and Conditions.

Table 8 provides a budget allocation plan for resilience enhancement using a linear utility function. As the baseline scenario, it presents the confidence levels for robustness and recovery abilities under budget allocations ranging from $2 billion to $3.5 billion. Under a budget

of less than \$2 billion, the amount is not sufficient, even with some probability, to meet the desired levels of robustness and recovery ability of the components, which are 0.7 (on a scale from 0 to 1) and 20 hours, respectively. When we reach a budget of \$3.5 billion, the desired levels are met with a confidence level of 1. This means that the budget allocation is guaranteed to meet the desired levels of robustness and recovery ability under any circumstances for each component. With a budget of \$3 billion, the confidence levels for robustness ability and recovery ability are 0.84 and 1, respectively. This indicates that there is a 16% chance of the constraint not being met for robustness ability. Additionally, the desired levels are loosened by 20% and tightened by 20%, respectively. When the desired levels are loosened, a budget of \$1 billion is adequate to meet the robustness and recovery abilities with confidence levels of 0.51 and 0.56. For this scenario, with a budget of \$3 billion, a confidence level of 1 is obtained for both the robustness and recovery abilities of the system. Table 8 demonstrates the effects of tightening the limits by 20%, which requires higher budgets to achieve similar confidence levels. Under this scenario, at least \$3.5 billion is required to meet these levels with a certain probability. Therefore, these results emphasize how varying budget constraints and resilience targets affect the overall robustness and recovery abilities of a system.

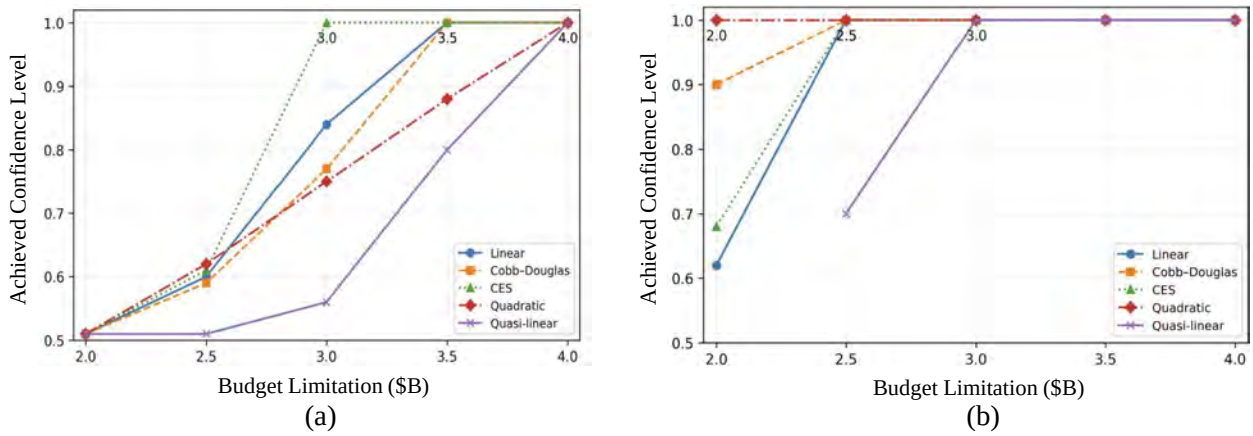

Figure 4: Robustness ability (a) and recovery ability (b) of the system considering different types of utility functions under the base case scenario.

Figure 4 reports the achieved confidence levels as a function of the budget limit B under alternative utility specifications. For robustness (left), CES ($\beta = 0.3$, $p = 0.7$) and Cobb–Douglas ($p = 0.7$) reach full confidence at lower budgets than Quadratic ($b_3 = 1, b_4 = 1$) and Quasi-linear ($\gamma_1 = 1, \gamma_2 = 1$). For recovery (right), Quadratic attains full confidence earlier, whereas Quasi-linear typically requires a higher budget to reach 1.00. The Linear utility uses $(\beta_1, \beta_2) = (0.5, 0.5)$. From a decision-making perspective, the figure provides a practical budgeting rule by indicating the minimum budget needed to attain a desired confidence level for robustness and recovery, and how this threshold shifts with the chosen utility specification.

Figure 5 displays how the functionality levels of system components change after allocating the budget to the components of the network. With a budget of \$3.5 billion, the system's confidence levels for both robustness and recovery reach 1.00. In the base case scenario, the desired robustness and recovery levels for the components are set at 0.7 (on a scale of 0 to

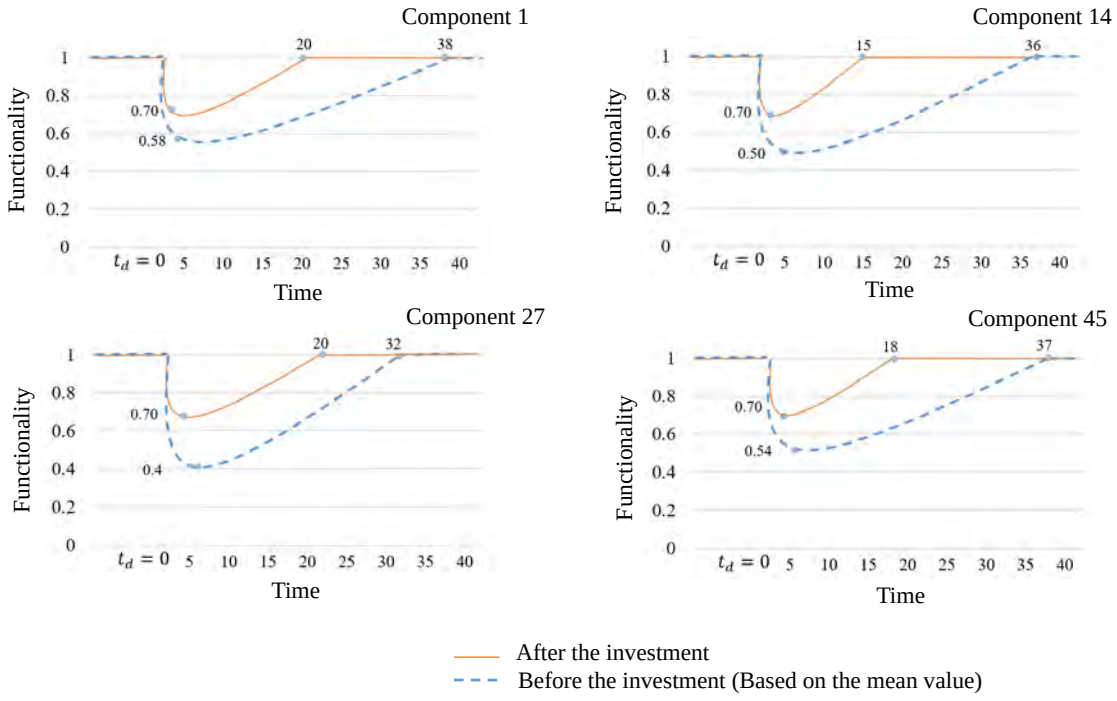

Figure 5: Resilience improvement of the components considering the base case scenario with a linear utility function under a budget of $3B.

1) and 20 hours, respectively. The results show that components 1, 14, 27, and 45 achieve the desired levels with confidence levels of 1.00, reflecting efficient budget allocation. For Component 1, the F_d value at time t_d was 0.58 and the recovery time was 38 hours before the investment, improving to 0.7 and 20 hours after the investment. Similarly, for Component 45, the F_d value at time t_d was 0.54, and the recovery time was 37 hours before the investment, which improved to 0.7 and 18 hours, respectively, after the investment. Thus, we can efficiently allocate the budget to the components by ensuring that system resilience remains within the predetermined range after adverse events, using the presented model.

4.3. Case 3: Transportation System

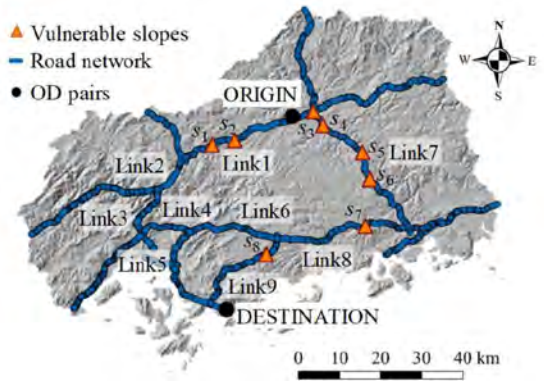

Figure 6: Transportation Network (He et al., 2025)

Figure 6 illustrates the transportation network in Hiroshima Prefecture, Japan, highlighting large areas identified as high-risk zones for rainfall-triggered landslides. Eight major vulnerable slopes, situated within buffer zones along the road network and exhibiting a higher likelihood of landslide occurrence, have been identified as potentially affecting road accessibility. Therefore, in this study, the system components consist of roads and bridges. Specifically, Links 1, 7, 8, and 9 correspond to Road 1, Road 7, Road 8, and Road 9, respectively, while Link 2 is assumed to contain Bridge 2, and Link 3 is assumed to contain Bridge 3, which are considered components of the system.

In the study by Lam et al. (2018), four damage states are defined for each component: d_{s_0}: no damage; d_{s_1}: limited damage with no lane closure; d_{s_2}: serious damage causing partial lane closure; and d_{s_3}: destroyed, resulting in full closure. Under an adverse hazard, Roads 8 and 9 are associated with d_{s_2}, while Roads 1 and 7 are associated with d_{s_3}. Bridge 3 is expected to be at d_{s_2}, and Bridge 2 at d_{s_3}. The degradation amount and recovery time of transportation components are assumed to follow a normal distribution.

Table 9 presents the corresponding means and standard deviations. Mean values for roads and bridges are adopted from Lam et al. (2018), which illustrates functional capacity loss and recovery time for bridge local scour and road section mudflow-blocking. In this context, functional capacity loss is interpreted as the reduction or loss of serviceability associated with partial or complete road closure of the affected component. Due to data limitations, the standard deviation is assumed to be 0.3 times the mean.

We incorporate the market value of components (V_i) into the utility functions through a scale factor (k_i), where k_i is assumed to be equal to $1/V_i$. For roads and bridges, this market value is approximated by their new construction cost, providing a consistent basis for representing the replacement value of these assets. The new construction cost is estimated at \$5,549,319 per mile for an undivided two-lane rural road (Florida Department of Transportation, 2024), including major cost components such as materials, labor, equipment, and at \$320 per square foot for a bridge (Florida Department of Transportation, 2025). It is assumed that Roads 1, 7, 8, and 9 are 20, 22, 20, and 15 miles long, respectively, and that each bridge has an area of 1,500 ft^2 In addition, a linear utility function is selected to reflect the risk perception of the decision maker, because it assumes a constant marginal utility and represents risk-neutral behavior.

4.3.1. Results

We consider three scenarios under linear utility functions. In the base case, the desired levels for component robustness and recovery ability are set to 0.8 (on a scale from 0 to 1) and 10 days, respectively. Then, we examine the outcomes when these targets are relaxed by 20%, resulting in a robustness level of 0.64 and a recovery time of 12 days, and when they are tightened by 20%, with a robustness level of 0.96 and a recovery time of 8 days. Detailed results derived from the mathematical model with a linear utility function are presented in Table 10.

Roads				
Damage States	Functional Degradation Amount [0,1]		Recovery Time (days)	
	Mean	Std. Dev.	Mean	Std. Dev.
d_{s_2}	0.50	0.15	7	2.1
d_{s_3}	1.00	0.30	15	4.5

Bridges				
Damage States	Functional Degradation Amount [0,1]		Recovery Time (days)	
	Mean	Std. Dev.	Mean	Std. Dev.
d_{s_2}	0.20	0.06	30	9
d_{s_3}	1.00	0.30	60	18

Table 9: Functional degradation amount and recovery time values for roads and bridges under different damage states.

Budget Limitation ($M)	Confidence Levels $(1-\alpha)$					
	Base Case		Loosened levels by 20%		Tightened levels by 20%	
	Robustness Ability	Recovery Ability	Robustness Ability	Recovery Ability	Robustness Ability	Recovery Ability
$200	0.71	0.50	1.00	0.72	–	–
$250	1.00	0.93	1.00	1.00	–	–
$300	1.00	1.00	1.00	1.00	1.00	0.92
$350	1.00	1.00	1.00	1.00	1.00	1.00

Note: "–" indicates that no feasible solution exists under the given budget.

Table 10: Confidence Levels for Robustness and Recovery Abilities under Different Budget Limitations and Conditions.

Table 10 presents the confidence levels for robustness and recovery abilities under different budget limitations and target conditions. In the base case scenario, a budget of $200M results in a moderate robustness confidence level of 0.71 and a relatively low recovery confidence level of 0.50, suggesting that the system's performance is constrained by limited resources. Increasing the budget to $250M significantly improves performance, with robustness confidence reaching 1.00 and recovery confidence increasing to 0.93, indicating near-complete satisfaction of the desired targets. At $300M and above, both robustness and recovery confidence levels reach 1.00, meeting all the base case performance requirements.

When the desired performance levels are loosened by 20%, the system's robustness confidence reaches 1.00 even at the lowest budget of $200M, while recovery confidence at this budget improves to 0.72. Further budget increases to $250M or more allow the recovery confidence to also reach 1.00, indicating that relaxed performance thresholds enable the system to achieve full confidence more easily across both metrics.

In contrast, when the performance levels are tightened by 20%, the system becomes infeasible at budgets of $200M and $250M for both robustness and recovery abilities, reflecting the greater difficulty in meeting stricter targets under constrained resources. At higher

budgets, robustness confidence maintains a perfect score of 1.00, while recovery confidence improves to 0.92 at \$300M and reaches full confidence at \$350M. These results emphasize the inherent trade-off between performance requirements and budget availability, where stricter targets necessitate substantially greater investment to achieve comparable confidence levels.

Components (i)	Road 1	Road 7	Road 8	Road 9	Bridge 2	Bridge 3
a_i	0.91	0.91	0.82	0.82	0.91	0.54
r_i	0.54	0.54	0.01	0.01	0.88	0.77
y_i	\$80,409,205	\$88,254,007	\$46,052,788	\$34,539,591	\$430,259	\$314,150

Table 11: Percentage improvement in absorption amount and recovery time, and investment amount for each component under a \$250M budget limitation for the base scenario.

Table 11 summarizes the percentage improvement in absorption amount and recovery time, along with the corresponding investment amounts, for each transportation component under a \$250M budget in the base scenario. Roads 1 and 7 demonstrate high levels of improvement in both robustness and recovery, receiving the largest shares of the investment budget. Roads 8 and 9 show slightly lower robustness improvements and minimal recovery enhancements, resulting in comparatively smaller allocations. Bridge 2, despite receiving one of the smallest shares of the budget, shows a high recovery improvement alongside a strong robustness gain. Bridge 3, with moderate improvements in both robustness and recovery, receives a mid-level investment.

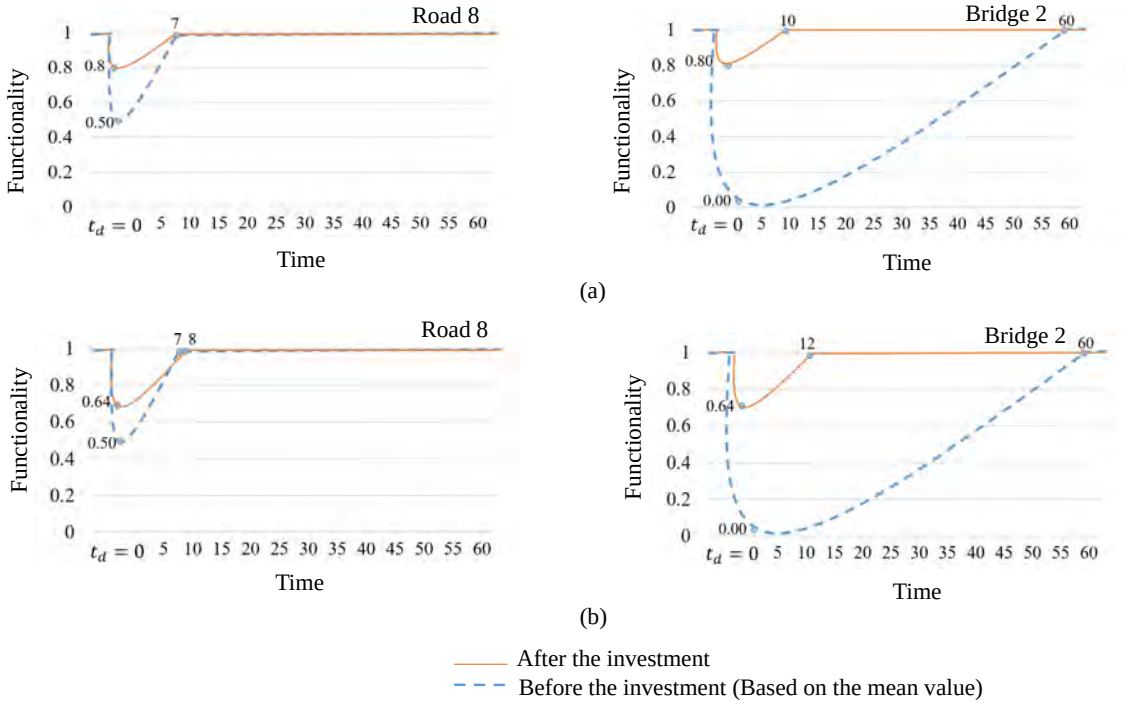

Figure 7: (a) Resilience improvement of the components considering the base case scenario under a budget of \$200M; (b) Resilience improvement of the components under the scenario with loosened levels by 20% under a budget of \$200M.

Figure 7 summarizes the post-allocation functionality trajectories for representative assets under a $200M budget. In both the base and loosened-level scenarios, the investment improves robustness at t_d and accelerates restoration for the most critical components, illustrating how the model prioritizes resilience gains under a binding budget constraint.

4.4. A Comparative Analysis of Results for Non-Convex Utility Functions

The linear, quadratic, and quasi-linear functions used in the case studies are convex, ensuring the guarantee of a global optimum. However, Cobb–Douglas and CES functions are inherently non-convex. We apply the successive convex approximation method to the power system test case under a $2 billion budget constraint for the Cobb–Douglas and CES utility functions. A comparison is made between the results obtained from the BARON solver and the SCA. The BARON solver was chosen for its capability to find solutions to challenging nonlinear optimization problems with global search capabilities. The results are presented in Table 12.

Utility function	β	p	Solver BARON			SCA		
			Robustness Ability	Recovery Ability	CPU (s)	Robustness Ability	Recovery Ability	CPU (s)
CES	0.3	0.7	0.51	0.68	42.580	0.51	0.68	0.012
	0.5	0.5	0.51	0.76	615.440	0.51	0.76	0.014
	0.7	0.3	0.51	0.846	9621.750	0.51	0.844	0.013
Cobb–Douglas		0.3	0.51	0.859	559.500	0.51	0.856	0.490
		0.5	0.51	0.90	7714.880	0.51	0.90	0.510
		0.7	0.51	0.91	583.730	0.51	0.91	0.740

Table 12: Comparison of results obtained from the BARON solver and SCA algorithm under CES and Cobb–Douglas utility functions.

Table 10 compares the results obtained from the CES utility function using two approaches: the BARON solver and the SCA algorithm. For different combinations of β and p parameters, the robustness ability remains constant at 0.51, while the recovery ability increases as β grows, indicating better recovery performance with higher β values. Although both methods yield identical robustness and recovery levels, the computation time differs drastically. BARON requires significantly longer CPU times, whereas SCA achieves convergence in less than 0.02 seconds, demonstrating its computational efficiency. This highlights that SCA can achieve similar solution quality with far lower computational cost.

The outcomes for the Cobb-Douglas function under similar parameter variations. The robustness ability again remains stable at 0.51 across all cases, while recovery ability increases as p rises, implying improved recovery performance with higher p. Similar to the CES results, BARON achieves comparable confidence levels but at the cost of very high CPU times whereas SCA provides nearly identical results within less than one second. Overall, the comparison shows that while both solvers deliver consistent robustness and recovery outcomes, SCA drastically reduces computation time, making it a more efficient and scalable approach.

4.5. Cross-Case Discussion

Across all three case studies, the framework yields consistent decision relevant patterns. First, decision-maker levers such as budget level, robustness–recovery prioritization weights, and desired robustness and recovery levels drive the largest shifts in achieved confidence and in the allocation split between robustness and recovery oriented actions. Second, optimal allocations often concentrate on a small subset of critical components, suggesting that resilience gains may be driven by prioritizing high impact assets rather than distributing resources uniformly. Third, the case studies indicate that allocation priorities respond meaningfully to changes in expected damage and expected recovery time, which helps practitioners calibrate and explain the plan using these mean inputs and underscores the importance of uncertainty-aware resilience planning. Finally, utility function choice serves as a portable calibration layer: different functional forms and parameter settings can alter how consistently plans meet robustness and recovery requirements, supporting context specific preference modeling without changing the core optimization structure.

5. Conclusion

Adverse events such as natural disasters, earthquakes, and floods can cause undesirable consequences, but resilience quantification can systematically assess and enhance system resilience and mitigate the devastating results. In this research, a chance-constrained model is developed for budget allocation decisions to maximize infrastructure system resilience, considering the uncertainty of extreme events by accounting for functional degradation amounts and recovery times. This model ensures that system resilience remains at desired levels with a specified confidence level under extreme conditions. Utility functions from economics, such as linear, Cobb–Douglas, and CES, are integrated to optimally allocate the budget across components. We derive the second-order cone programming equivalents of chance constraints under both normal and uniform distributions of the uncertain parameters. This framework is also broadened by incorporating various probability distributions with some modifications. Moreover, a successive convex approximation algorithm incorporating first-order Taylor expansion is employed to convexify the non-convex utility formulation. Numerical results demonstrate that this method substantially improves computational efficiency and reduces CPU time. The effectiveness of the proposed algorithm and the overall framework is validated through three case studies conducted on generic, power, and transportation systems. Using the case studies, we demonstrated that the minimum budget required to achieve specific robustness and recovery targets for each component under uncertainty can be determined with a high level of confidence. The findings also provide insights into optimal resource allocation among components, enabling the system to effectively withstand and recover from adverse events. In the future, other factors, such as redundancy and resourcefulness, can also be incorporated into the optimization model.

Acknowledgment

This work was partially supported by the National Science Foundation (NSF) under grant ECCS-2338158 and an Early-Career Research Fellowship from the Gulf Research Program

of the National Academies of Sciences, Engineering, and Medicine (NASEM) under SCON-10001218. The content is solely the authors' responsibility and does not necessarily represent the official views of the Gulf Research Program of NASEM.

References

Agterberg, F. (2014). Probability and statistics. In *Geomathematics: Theoretical Foundations, Applications and Future Developments* chapter 2. (pp. 41–72). Cham: Springer International Publishing. https://doi.org/10.1007/978-3-319-06874-9_2.

Ahmadian, N., Lim, G. J., Cho, J., & Bora, S. (2020). A quantitative approach for assessment and improvement of network resilience. *Reliability Engineering & System Safety*, *200*, 106977. https://doi.org/10.1016/j.ress.2020.106977.

Arif, A., Ma, S., Wang, Z., Wang, J., Ryan, S. M., & Chen, C. (2018). Optimizing service restoration in distribution systems with uncertain repair time and demand. *IEEE Transactions on Power Systems*, *33*, 6828–6838. doi:https://doi.org/10.1109/TPWRS.2018.2855102.

Arrow, K. J., Chenery, H. B., Minhas, B. S., & Solow, R. M. (1961). Capital-labor substitution and economic efficiency. *The review of Economics and Statistics*, *43*, 225–250.

Ashokaraju, D., Ramamoorthy, M. L., Simon, D. et al. (2026). A time-coupled multi-objective distributionally robust chance-constrained framework for grid resilience enhancement using mobile emergency generators. *Scientific Reports*, *16*, 6204. https://doi.org/10.1038/s41598-026-37197-4.

Bavaghar Zaeimi, M., & Abbas Rassafi, A. (2021). Designing an integrated municipal solid waste management system using a fuzzy chance-constrained programming model considering economic and environmental aspects under uncertainty. *Waste Management*, *125*, 268–279. https://doi.org/10.1016/j.wasman.2021.02.047.

Bazaraa, M. S., Sherali, H. D., & Shetty, C. M. (2013). *Nonlinear programming: theory and algorithms*. John wiley & sons.

Bilsel, R. U., & Ravindran, A. (2011). A multiobjective chance constrained programming model for supplier selection under uncertainty. *Transportation Research Part B: Methodological*, *45*, 1284–1300. https://doi.org/10.1016/j.trb.2011.02.007.

Biswas, S., Singh, M. K., & Centeno, V. A. (2021). Chance-constrained optimal distribution network partitioning to enhance power grid resilience. *IEEE Access*, *9*, 42169–42181. https://doi.org/10.1109/ACCESS.2021.3065577.

Bruneau, M., Chang, S. E., Eguchi, R. T., Lee, G. C., O'Rourke, T. D., Reinhorn, A. M., Shinozuka, M., Tierney, K., Wallace, W. A., & von Winterfeldt, D. (2003). A framework to quantitatively assess and enhance the seismic resilience of communities. *Earthquake Spectra*, *19*, 733–752. https://doi.org/10.1193/1.1623497.

Calafiore, G. C., & Ghaoui, L. E. (2006). On distributionally robust chance-constrained linear programs. *Journal of Optimization Theory and Applications*, *130*, 1–22. https://doi.org/10.1007/s10957-006-9084-x.

Charnes, A., & Cooper, W. W. (1959). Deterministic equivalents for optimizing and satisficing under chance constraints. *Operations Research*, *11*, 18–39. https://doi.org/10.1287/opre.11.1.18.

De Luca, P. (2018). Utility function approach. In *Analytical Corporate Valuation: Fundamental Analysis, Asset Pricing, and Company Valuation* chapter 4. (pp. 119–164). Cham: Springer International Publishing. https://doi.org/10.1007/978-3-319-93551-5_4.

DeSantis, D., James, B. D., Houchins, C., Saur, G., & Lyubovsky, M. (2021). Cost of long-distance energy transmission by different carriers. *IScience*, *24*, 103495. https://doi.org/10.1016/j.isci.2021.103495.

Ermoliev, Y., Ermolieva, T., MacDonald, G., & Norkin, V. (2000). Stochastic optimization of insurance portfolios for managing exposure to catastrophic risks. *Annals of Operations Research*, *99*, 207–225. https://doi.org/10.1023/A:1019244405392.

Fattahi, M., Govindan, K., & Maihami, R. (2020). Stochastic optimization of disruption-driven supply chain network design with a new resilience metric. *International Journal of Production Economics*, *230*, 107755. https://doi.org/10.1016/j.ijpe.2020.107755.

Florida Department of Transportation (2024). Cost per mile models reports. https://www.fdot.gov/programmanagement/estimates/reports/cost-per-mile-models-reports. [accessed 11 August 2025].

Florida Department of Transportation (2025). *2025 Structures Manual*. Technical Report FDOT Structures Manual Florida Department of Transportation. URL: https://fdotwww.blob.core.windows.net/sitefinity/docs/default-source/structures/structuresmanual/currentrelease/2025/2025-structures-manual.pdf?sfvrsn=f658fd25_1 [accessed 11 August 2025].

Francis, R., & Bekera, B. (2014). A metric and frameworks for resilience analysis of engineered and infrastructure systems. *Reliability Engineering & System Safety*, *121*, 90–103. https://doi.org/10.1016/j.ress.2013.07.004.

He, Z., Akiyama, M., Firdaus, P. S., Huang, Y., Frangopol, D. M., & Aoki, K. (2025). Probabilistic connectivity assessment of road networks exposed to spatially correlated rainfall-triggered landslides. *Reliability Engineering & System Safety*, *257*, 110800. https://doi.org/10.1016/j.ress.2025.110800.

Hou, H., Tang, J., Zhang, Z., Wu, X., Wei, R., Wang, L., & He, H. (2023). Stochastic pre-disaster planning and post-disaster restoration to enhance distribution system resilience during typhoons. *Energy Conversion and Economics*, *4*, 346–363. https://doi.org/10.1049/enc2.12098.

Huang, R., Qu, S., & Liu, Z. (2023). Two-stage distributionally robust optimization model for warehousing-transportation problem under uncertain environment. *Journal of Industrial & Management Optimization*, *19*, 1–20. https://doi.org/10.3934/jimo.2022218.

Izadikhah, M., Azadi, M., Toloo, M., & Hussain, F. K. (2021). Sustainably resilient supply chains evaluation in public transport: A fuzzy chance-constrained two-stage dea approach. *Applied Soft Computing*, *113*, 107879. https://doi.org/10.1016/j.asoc.2021.107879.

Jayakumar, K., & Sankaran, K. K. (2016). On a generalisation of uniform distribution and its properties. *Statistica*, *76*, 83–91. https://doi.org/10.6092/issn.1973-2201/6090.

Knabb, R. D., Rhome, J. R., & Brown, D. P. (2005). *Tropical Cyclone Report: Hurricane Katrina, 23-30 August 2005*. Technical Report National Hurricane Center. https://www.nhc.noaa.gov/data/tcr/AL122005_Katrina.pdf [accessed 8 October 2024].

Lagoa, C. M., Li, X., & Sznaier, M. (2005). Probabilistically constrained linear programs and risk-adjusted controller design. *SIAM Journal on Optimization*, *15*, 938–951. https://doi.org/10.1137/S1052623403430099.

Lam, J. C., Adey, B. T., Heitzler, M., Hackl, J., Gehl, P., van Erp, N., D'Ayala, D., van Gelder, P., & Hurni, L. (2018). Stress tests for a road network using fragility functions and functional capacity loss functions. *Reliability Engineering & System Safety*, *173*, 78–93. https://doi.org/10.1016/j.ress.2018.01.015.

Li, Z., Jin, C., Hu, P., & Wang, C. (2019). Resilience-based transportation network recovery strategy during emergency recovery phase under uncertainty. *Reliability Engineering & System Safety*, *188*, 503–514. https://doi.org/10.1016/j.ress.2019.03.052.

Lindsey, K. E. (2015). *Transmission emergency restoration systems for public power*. Technical Report Lindsey Manufacturing. https://lindsey-usa.com/wp-content/uploads/2015/10/07T-005-ERS-PUBLIC-POWER.pdf [accessed 24 March 2025].

Miller, B. L., & Wagner, H. M. (1965). Chance constrained programming with joint constraints. *Operations Research*, *13*, 930–945. https://doi.org/10.1287/opre.13.6.930.

Montgomery, D. C., & Runger, G. C. (2020). *Applied statistics and probability for engineers*. John wiley & sons.

Najarian, M., & Lim, G. J. (2019). Design and assessment methodology for system resilience metrics. *Risk Analysis*, *39*, 1885–1898. https://doi.org/10.1111/risa.13274.

Najarian, M., & Lim, G. J. (2020). Optimizing infrastructure resilience under budgetary constraint. *Reliability Engineering & System Safety*, *198*, 106801. https://doi.org/10.1016/j.ress.2020.106801.

National Institute of Standards and Technology (2017). *Guide Brief 13 - Resilience Gaps: Identifying and Prioritizing Closure of Resilience Gaps*. Special Publication NIST SP 1190GB-13 National Institute of Standards and Technology Gaithersburg, MD. URL: https://doi.org/10.6028/NIST.SP.1190GB-13 [accessed 24 March 2025].

Nemirovski, A., & Shapiro, A. (2007). Convex approximations of chance constrained programs. *SIAM Journal on Optimization*, *17*, 969–996. https://doi.org/10.1137/050622328.

Ouyang, M., Dueñas-Osorio, L., & Min, X. (2012). A three-stage resilience analysis framework for urban infrastructure systems. *Structural Safety*, *36-37*, 23–31. https://doi.org/10.1016/j.strusafe.2011.12.004.

Palomar, D. P. (2025). *Portfolio Optimization: Theory and Application*. Cambridge, UK: Cambridge University Press.

Panteli, M., Pickering, C., Wilkinson, S., Dawson, R., & Mancarella, P. (2017). Power system resilience to extreme weather: Fragility modeling, probabilistic impact assessment, and adaptation measures. *IEEE Transactions on Power Systems*, *32*, 3747–3757. https://doi.org/10.1109/TPWRS.2016.2641463.

Park, S., & Shin, H. (2022). A proactive microgrid management strategy for resilience enhancement based on nested chance constrained problems. *Applied Sciences*, *12*, 12649. https://doi.org/10.3390/app122412649.

Pintér, J. (1989). Deterministic approximations of probability inequalities. *ZOR - Methods and Models of Operations Research*, *33*, 219–239. https://doi.org/10.1007/BF01423332.

Prékopa, A. (1995). *Stochastic Programming*. Mathematics and Its Applications. Springer Dordrecht. https://doi.org/10.1007/978-94-017-3087-7.

Prékopa, A. (1973). Contributions to the theory of stochastic programming. *Mathematical Programming*, *4*, 202–221. https://doi.org/10.1007/BF01584661.

Reed, D. A., Kapur, K. C., & Christie, R. D. (2009). Methodology for assessing the resilience of networked infrastructure. *IEEE Systems Journal*, *3*, 174–180. https://doi.org/10.1109/JSYST.2009.2017396.

Ren, F., Zhao, T., Jiao, J., & Hu, Y. (2017). Resilience optimization for complex engineered systems based on the multi-dimensional resilience concept. *IEEE Access*, *5*, 19352–19362. https://doi.org/10.1109/ACCESS.2017.2755043.

Rohatgi, A. (2024). Webplotdigitizer. https://automeris.io. Version 5.2.

Scutari, G., & Sun, Y. (2018). Parallel and distributed successive convex approximation methods for big-data optimization. In F. Facchinei, & J.-S. Pang (Eds.), *Multi-agent Optimization* (pp. 141–308). Cham: Springer volume 2224 of *Lecture Notes in Mathematics*. https://doi.org/10.1007/978-3-319-97142-1_3.

Shabazbegian, V., Ameli, H., Ameli, M. T., Strbac, G., & Qadrdan, M. (2021). Co-optimization of resilient gas and electricity networks; a novel possibilistic chance-constrained programming approach. *Applied Energy*, *284*, 116284. https://doi.org/10.1016/j.apenergy.2020.116284.

Shi, Q., Li, F., Dong, J., Olama, M., Wang, X., Winstead, C., & Kuruganti, T. (2022). Co-optimization of repairs and dynamic network reconfiguration for improved distribution system resilience. *Applied Energy*, *318*, 119245. https://doi.org/10.1016/j.apenergy.2022.119245.

Shuai, H., Li, F., She, B., Wang, X., & Zhao, J. (2023). Post-storm repair crew dispatch for distribution grid restoration using stochastic Monte Carlo tree search and deep neural networks. *International Journal of Electrical Power & Energy Systems*, *144*, 108477. https://doi.org/10.1016/j.ijepes.2022.108477.

Song, Y., & Li, R. (2022). System resilience distribution identification and analysis based on performance processes after disruptions. *PLOS ONE*, *17*, e0276908. https://doi.org/10.1371/journal.pone.0276908.

U.S. Geological Survey (2024). M6.7 January 17, 1994 Northridge, California earthquake. https://www.usgs.gov/centers/earthquake-science-center/science/m67-january-17-1994-northridge-california-earthquake. [accessed 28 August 2025].

Varian, H. R. (2010). *Intermediate Microeconomics: A Modern Approach*. (8th ed.). New York: W. W. Norton & Company.

Wang, F., Tian, J., Shi, C., Ling, J., Chen, Z., & Xu, Z. (2024). A multi-stage quantitative resilience analysis and optimization framework considering dynamic decisions for urban infrastructure systems. *Reliability Engineering & System Safety*, *243*, 109851. https://doi.org/10.1016/j.ress.2023.109851.

Wang, H., Xing, H., Luo, Y., & Zhang, W. (2023). Optimal scheduling of micro-energy grid with integrated demand response based on chance-constrained programming. *International Journal of Electrical Power & Energy Systems*, *144*, 108602. https://doi.org/10.1016/j.ijepes.2022.108602.

Xu, L., Feng, K., Lin, N., Perera, A., Poor, H. V., Xie, L., Ji, C., Sun, X. A., Guo, Q., & O'Malley, M. (2024). Resilience of renewable power systems under climate risks. *Nature Reviews Electrical Engineering*, *1*, 53–66. https://doi.org/10.1038/s44287-023-00003-8.

Yodo, N., & Wang, P. (2016). Engineering resilience quantification and system design implications: A literature survey. *Journal of Mechanical Design*, *138*, 111408. https://doi.org/10.1115/1.4034223.

Zaghian, M., Lim, G. J., & Khabazian, A. (2018). A chance-constrained programming framework to handle uncertainties in radiation therapy treatment planning. *European Journal of Operational Research*, *266*, 736–745. https://doi.org/10.1016/j.ejor.2017.10.018.

Zhang, C., Kong, J., & Simonovic, S. P. (2018). Restoration resource allocation model for enhancing resilience of interdependent infrastructure systems. *Safety Science*, *102*, 169–177. https://doi.org/10.1016/j.ssci.2017.10.014.

Appendix A: Proof of Proposition 1.

Proof. Consider the chance constraint $P\{x^T a_i \leq b_i\} \geq 1 - \alpha$. Let the uncertain parameter a_i be affinely dependent on the random vector Δa_i.

$$a_i = a_i^0 + \Delta a_i \quad \text{for} \quad i = 1, 2, \ldots, k$$

where a^0 corresponds the nominal value of the random parameters a_i, and Δa_i follows a symmetric log-concave probability distribution. If the uncertain parameters follow a log-concave, symmetric distribution and the risk levels are within the range $0 \leq \alpha \leq 0.5$, the probabilistic constraint is convex (Lagoa et al., 2005; Nemirovski & Shapiro, 2007; Prékopa, 1995). As a result, the following chance constraint is regarded as convex.

$$P\{x^T(a_0 + \Delta a) \leq b\} \geq 1 - \alpha$$

Consider chance constraints (5) and (8)). Assume the uncertain parameters A_i and T_i depend affinely on the random variables ΔA_i and ΔT_i, both of which follow normal distributions.

$$A_i = A_i^0 + \Delta A_i \quad \text{for} \quad i = 1, 2, \ldots, k$$

$$T_i = T_i^0 + \Delta T_i \quad \text{for} \quad i = 1, 2, \ldots, k$$

where the nominal values of the random parameters A_i and T_i are represented by A^0 and T^0, respectively. Both ΔA_i and ΔT_i have log-concave symmetric probability density functions. Consequently, the chance constraints (5) and (8) can be expressed as follows:

$$P\{(A_i^0 + \Delta A_i)(1 - a_i) \leq Ro - Qd\} \geq 1 - \alpha$$

$$P\{(T_i^0 + \Delta T_i)(1 - r_i) \leq Qt\} \geq 1 - \alpha$$

Therefore, the chance constraints (5) and (8) are convex when $\alpha \in [0, 0.5]$ under the normal distribution of the uncertain parameters. Note that the normal distribution is both log-concave and symmetric.

Appendix B: Proof of Proposition 2.

Proof. Given the assumption of a normal distribution, the standardized version of $\tilde{H}_i(a_i)$ is formulated as:

$$\tilde{Z}_i = \frac{\tilde{H}_i(a_i) - E(\tilde{H}_i(a_i))}{\sigma(\tilde{H}_i(a_i))}$$

The chance constraint (5) can be reformulated as follows:

$$P\left\{\frac{\tilde{H}_i(a_i) - E(\tilde{H}_i(a_i))}{\sigma(\tilde{H}_i(a_i))} \leq \frac{(R_0 - Q_d) - E(\tilde{H}_i(a_i))}{\sigma(\tilde{H}_i(a_i))}\right\} \geq 1 - \alpha_d$$

$$P\left\{\tilde{Z}_i \leq \frac{(R_0 - Q_d) - E(\tilde{H}_i(a_i))}{\sigma(\tilde{H}_i(a_i))}\right\} \geq 1 - \alpha_d$$

$$\frac{(R_0 - Q_d) - E(\tilde{H}_i(a_i))}{\sigma(\tilde{H}_i(a_i))} \geq \Phi^{-1}(1 - \alpha_d)$$

from which constraint (18) is obtained. With the assumption of a normal distribution, $\tilde{L}_i(r_i)$ is standardized as follows:

$$\tilde{Z}_i = \frac{\tilde{L}_i(r_i) - E(\tilde{L}_i(r_i))}{\sigma(\tilde{L}_i(r_i))}$$

The chance constraint (8) can be reformulated as follows:

$$P\left\{\frac{\tilde{L}_i(r_i) - E(\tilde{L}_i(r_i))}{\sigma(\tilde{L}_i(r_i))} \leq \frac{Q_t - E(\tilde{L}_i(r_i))}{\sigma(\tilde{L}_i(r_i))}\right\} \geq 1 - \alpha_t$$

$$P\left\{\tilde{Z}_i \leq \frac{Q_t - E(\tilde{L}_i(r_i))}{\sigma(\tilde{L}_i(r_i))}\right\} \geq 1 - \alpha_t$$

$$\frac{Q_t - E(\tilde{L}_i(r_i))}{\sigma(\tilde{L}_i(r_i))} \geq \Phi^{-1}(1 - \alpha_t)$$

from which constraint (19) is obtained.

Appendix C: Proof of Proposition 3.

Proof. Assume the uncertain parameters A_i and T_i depend affinely on the random variables ΔA_i and ΔT_i. $A_i - E(A_i)$ and $T_i - E(T_i)$ follow a uniform distribution defined as:

$$A_i - E(A_i) = A_i - A_i^0 = \Delta A_i$$

$$T_i - E(T_i) = T_i - T_i^0 = \Delta T_i$$

ΔA_i and ΔT_i are regarded as being uniformly distributed within the ellipsoid $\varepsilon = \{\xi = Qz : \|z\| \leq 1\}$, which is characterized by a log-concave distribution function. The proof follows a similar method to Proposition 1. Consequently, the feasible region defined by the chance constraints is convex (Lagoa et al., 2005; Nemirovski & Shapiro, 2007; Prékopa, 1995).

Appendix D: Proof of Proposition 4.

Proof. Chance constraints can be reformulated using the mean and standard deviation as follows.

$$P\left\{\frac{\tilde{H}_i(a_i) - E(\tilde{H}_i(a_i))}{\sigma(\tilde{H}_i(a_i))} \leq \frac{(R_0 - Q_d) - E(\tilde{H}_i(a_i))}{\sigma(\tilde{H}_i(a_i))}\right\} \geq 1 - \alpha_d \tag{31}$$

$$P\left\{\frac{\tilde{L}_i(r_i) - E(\tilde{L}_i(r_i))}{\sigma(\tilde{L}_i(r_i))} \leq \frac{Q_t - E(\tilde{L}_i(r_i))}{\sigma(\tilde{L}_i(r_i))}\right\} \geq 1 - \alpha_t \tag{32}$$

The uniform distribution over the ellipsoid $\mathcal{E} = \{\xi = \nu\Gamma_f z : \|z\| \leq 1\}$ is generated through scaling a uniformly distributed vector ω from the unit Euclidean ball by $\nu\Gamma_f$. Thus, if $A_i - E(A_i)$ is uniformly distributed in $\mathcal{E}$, it can be written as:

$$A_i - E(A_i) = \nu\Gamma_f\omega,$$

where $\omega \in \mathbb{R}^{n+1}$ follows a uniform distribution within the set $\{z : \|z\| \leq 1\}$. Thus, we have

$$\tilde{H}_i(a_i) - E(\tilde{H}_i(a_i)) = (\nu\Gamma_f h)^T a_i$$

The probability distribution of $\left[\tilde{H}_i(a_i) - E(\tilde{H}_i(a_i))\right]/\nu\sigma(\tilde{H}_i(a_i))$ is given by Calafiore & Ghaoui (2006)

$$\frac{S_n}{nV_{n+1}}\left(1 - \xi^2\right)^{n/2}, \quad \xi \in [-1, 1].$$

The expression for $V_n = \pi^{n/2}/\Gamma(n/2+1)$, in which $\Gamma(\cdot)$ represents the standard gamma function, and S_n is equal to nV_n. The symmetric density gives the cumulative probability function $\Psi(\xi)$ for $\xi \in [-1, 1]$ as

$$\Psi(\xi) = \frac{1}{2} + \left(\frac{1}{2}\right)\text{sign}(\xi)\int_0^{|\xi|}(2S_n/nV_{n+1})(1 - y^2)^{n/2}\,dy.$$

By substituting $z = y^2$, the expression becomes

$$\Psi(\xi) = \frac{1}{2} + \frac{1}{2}\text{sign}(\xi)\Psi_{\text{beta}}(\xi^2),$$

where Ψ_{beta} represents the cumulative distribution function of a beta distribution with parameters $(1/2, n/2+1)$.

Using Equation (31), we have

$$\Psi\left\{\frac{(R_0 - Q_d) - \mathbb{E}(\tilde{H}_i(a_i))}{\nu\sigma(\tilde{H}_i(a_i))}\right\} \geq \alpha_d.$$

Next, substituting the function $\Psi(.)$, we get

$$\frac{1}{2} + \frac{1}{2}\text{sign}(Y_T)\Psi_{\text{beta}}\left(Y_T^{-2}\right) \geq \alpha_d,$$

where $Y_T = \left\{\frac{(R_0 - Q_d) - \mathbb{E}(\tilde{H}_i(a_i))}{\nu\sigma(\tilde{H}_i(a_i))}\right\}$.

Thus, it follows

$$\operatorname{sign}(Y_T)\Psi_{\text{beta}}(Y_T^{-2}) \geq 2\alpha_d - 1.$$

This leads to the inequality

$$\left(\frac{(R_0 - Q_d) - \mathbb{E}(\tilde{H}_i(a_i))}{\nu\sigma(\tilde{H}_i(a_i))}\right)^2 \geq \Psi_{\text{beta}}^{-1}(1 - 2\alpha_d),$$

and finally

$$\mathbb{E}(\tilde{H}_i(a_i)) + \nu\sqrt{\Psi_{\text{beta}}^{-1}(1 - 2\alpha_d)}\sigma(\tilde{H}_i(a_i)) \leq (R_0 - Q_d).$$

This completes the proof for Equation (23). A similar approach can be applied for the Equation (24).

Appendix E: Input Data for Numerical Analysis

Components	Degradation Amount		Recovery Time	
	μ_{A_i}	σ_{A_i}	μ_{T_i}	σ_{T_i}
i=1	0.5	0.05	100	17
i=2	0.4	0.04	75	13
i=3	0.6	0.05	80	15
i=4	0.8	0.06	85	5
i=5	0.5	0.02	70	14
i=6	0.6	0.03	75	8
i=7	0.7	0.04	60	12
i=8	0.9	0.05	110	10
i=9	0.4	0.05	55	5
i=10	0.5	0.06	70	7

Table 13: Degradation amount and recovery time follow normal distributions $N(\mu_{A_i}, \sigma_{A_i})$ and $N(\mu_{T_i}, \sigma_{T_i})$, respectively.

Components	Degradation Amount		Recovery Time	
	a_{A_i}	b_{A_i}	a_{T_i}	b_{T_i}
i=1	0.35	0.65	49	151
i=2	0.28	0.52	36	114
i=3	0.45	0.75	35	125
i=4	0.62	0.98	70	100
i=5	0.44	0.56	28	112
i=6	0.51	0.69	51	99
i=7	0.58	0.82	24	96
i=8	0.75	1.05	80	140
i=9	0.25	0.55	40	70
i=10	0.32	0.68	49	91

Table 14: Degradation amount and recovery time follow uniform distributions $U(a_{A_i}, b_{A_i})$ and $U(a_{T_i}, b_{T_i})$, respectively.

Appendix F: Resilience Improvements in Case 1 (Illustrative System)

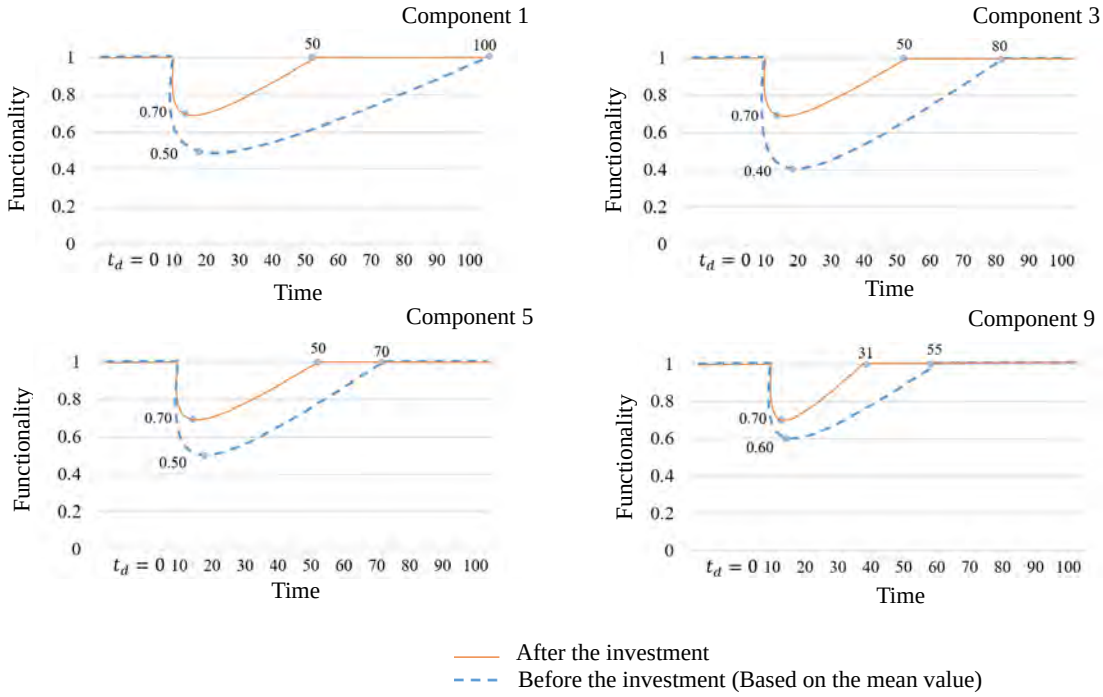

Figure 8: Resilience improvement of the components under uniform distribution with a linear utility function under a budget of $65,000.